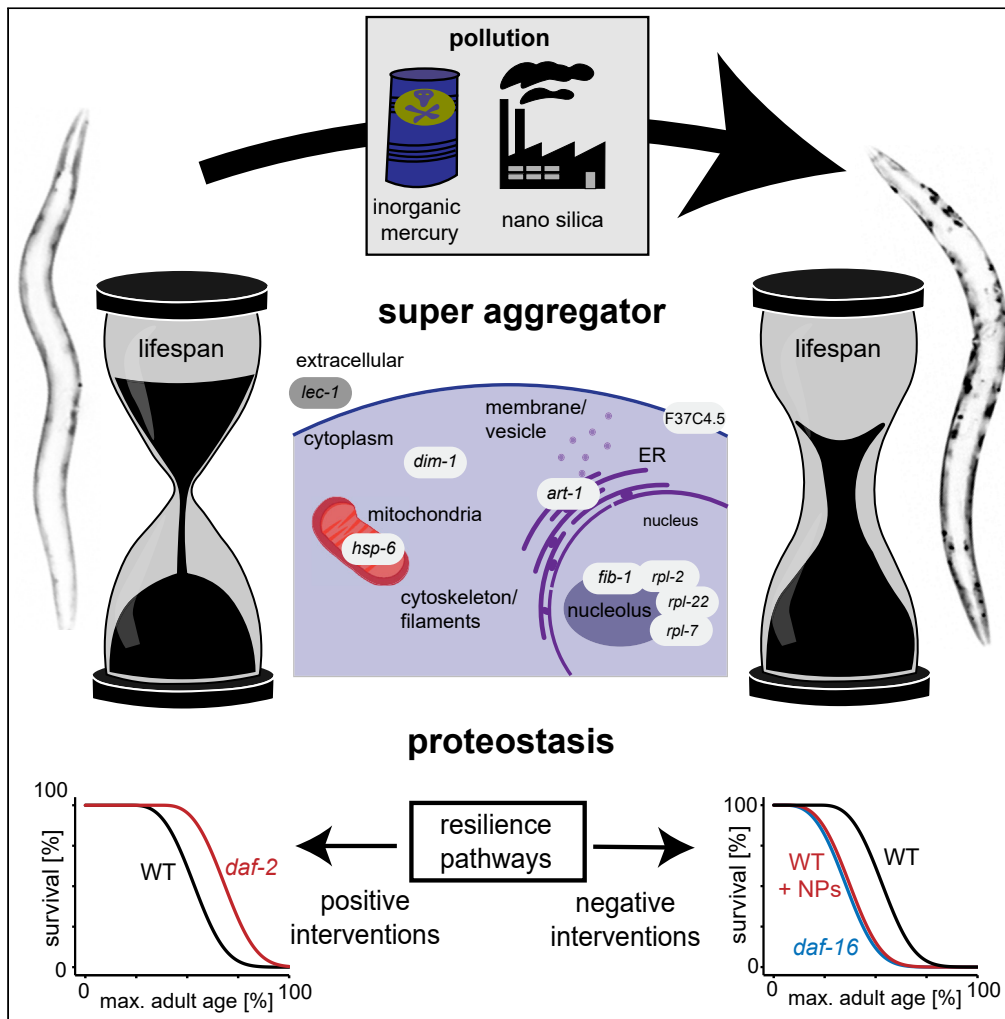**Article**

Pollutants corrupt resilience pathways of aging in the nematode *C. elegans*

Andrea Scharf,
Annette Limke,
Karl-Heinz Guehrs,
Anna von Mikecz

scharfa@uni-duesseldorf.de

Highlights

Two candidate pollutants, iHg, and nanosilica, reduce lifespans in *C. elegans*

iHg and silica NPs induce premature aggregation phenotypes in *C. elegans*

Pollutants-induced premature and intrinsic aging share nine super aggregation proteins

Reducing pollution is important for an effective strategy to support healthy aging

Article

Pollutants corrupt resilience pathways of aging in the nematode *C. elegans*

Andrea Scharf,[1,2,3,5,*] Annette Limke,[1] Karl-Heinz Guehrs,[4] and Anna von Mikecz[1]

SUMMARY

Delaying aging while prolonging health and lifespan is a major goal in aging research. One promising strategy is to focus on reducing negative interventions such as pollution and their accelerating effect on age-related degeneration and disease. Here, we used the short-lived model organism *C. elegans* to analyze whether two candidate pollutants corrupt general aging pathways. We show that the emergent pollutant silica nanoparticles (NPs) and the classic xenobiotic inorganic mercury reduce lifespan and cause a premature protein aggregation phenotype. Comparative mass spectrometry revealed that increased insolubility of proteins with important functions in proteostasis is a shared phenotype of intrinsic- and pollution-induced aging supporting the hypothesis that proteostasis is a central resilience pathway controlling lifespan and aging. The presented data demonstrate that pollutants corrupt intrinsic aging pathways. Reducing pollution is, therefore, an important step to increasing healthy aging and prolonging life expectancies on a population level in humans and animals.

INTRODUCTION

Aging is a common risk factor for morbidity and mortality in modern human society. To prolong life and reduce age-related diseases, millions of dollars are invested into understanding aging and developing effective therapeutics (Partridge et al., 2018). However, these efforts have been made without the consideration of another challenge: global pollution. Environmental pollution is a likely compounding factor in healthy aging as genetic and environmental factors contribute to aging, age-related changes, and death (Kenyon, 2010; Sorrentino et al., 2014; Vermeulen et al., 2020). The Lancet Commission on Pollution and Health reported that pollution is the number one cause of environmentally induced diseases and premature death (Landrigan et al., 2018). Air, water, and soil pollution caused an estimated 9 million premature deaths worldwide in 2015 (Forouzanfar et al., 2016). The actual number of deaths may be even higher owing to many emerging chemicals such as nanoparticles (NPs) or endocrine disruptors that have not yet been studied for their effects. Another neglected aspect in the evaluation of pollution costs is a pollution-induced decline in quality of life or health span that is not directly linked to a specific disease or death. In summary, pollution is an understudied negative aging intervention that counteracts healthy aging and reduces life expectancies.

To successfully promote longer health- and lifespan in humans, a comprehensive analysis of the negative interventions from the pollutome, which includes all pollutants and sources of exposure, would be required in addition to the development of therapeutic strategies for anti-aging interventions. However, a large number of pollutants in the pollutome limits this analysis in the human population. In addition, pollutants reflect manufacturing trends over time; therefore, old and emergent pollutants affect the overall composition of the pollutome. For example, inorganic mercury (iHg) represents an "old" pollutant as its concentrations in oceans and soils have been highly elevated owing to mining and fossil-fuel combustion for at least 150 years (Streets et al., 2011). Environmental mercury peaked around 1900 owing to the North American Gold/Silver Rush and rose again in 1950 with the rise in coal combustion and artisanal gold production (Streets et al., 2011). Since 1950, the chemical industry alone has added more than 150,000 newly synthesized chemicals (Landrigan et al., 2018), and most of these are not systematically analyzed nor are their biological interactions known. Among these, industrial nanoparticles (e.g., silica NPs) experienced mass production at the beginning of the 21st century highlighted by the announcement of the National Nanotechnology Initiative in the United States (Roco, 2003).

[1]IUF – Leibniz Research Institute for Environmental Medicine GmbH, Duesseldorf 40225, Germany

[2]Department of Developmental Biology, Washington University School of Medicine, St. Louis, MO 63110, USA

[3]Department of Biological Sciences, Missouri University of Science and Technology, Rolla, MO 65409, USA

[4]CF Proteomics, FLI-Leibniz-Institute on Aging -Fritz-Lipman-Institute (FLI), Jena 07745, Germany

[5]Lead contact

*Correspondence: scharfa@uni-duesseldorf.de

https://doi.org/10.1016/j.isci.2022.105027

The number and compositional complexity of pollutants complicate strategies that seek to understand the effects of the pollutome on human aging. A more feasible strategy is to take advantage of short-lived model organisms to analyze prominent representative "old versus emerging" pollutants on general aging resilience pathways impacted by negative and positive interventions.

Caenorhabditis elegans is a free-living nematode roundworm that thrives in microbe-rich habitats on rotting plant material. Its short life cycle has made *C. elegans* one of the supermodel organisms of current biomedicine especially in aging research (Tissenbaum, 2015). Under abundant growth conditions, a sequence of four larval stages is completed within approximately 2.5 days followed by a hermaphrodite adult stage lasting 2 to 3 weeks (Corsi et al., 2015). A plethora of genes regulates the aging of the adult worm, including the insulin/IGF-1-like signaling pathway identified in long-lived *daf-2* (insulin-like growth factor 1, IGF-1) and short-lived *daf-16* (FOXO transcription factor) mutants (Kenyon et al., 1993; Kenyon, 2010). The IGF signaling pathway influences the longevity of adult worms as well as aging processes that manifest through the degeneration of neural connectivity, reduced neural signaling, amyloid protein aggregation, and acceleration of neuromuscular defects (Collins et al., 2008; Kenyon, 2010; Walther et al., 2015). Notably, the genes of the aging pathways are largely conserved between *C. elegans*, *Drosophila melanogaster*, mice, and humans (Kaletta and Hengartner, 2006; Kenyon, 2010). In addition to its prominent role in aging research, *C. elegans* is an excellent model organism to study pollutant exposure in the laboratory (von Mikecz, 2018; von Mikecz and Scharf, 2022). One reason that makes *C. elegans* so suitable for this kind of study is their natural habitat on decaying plant material in the soil. In this habitat, *C. elegans* are exposed to pollutants that accumulate in biomaterial and in the soil, which can also be described as environmental sinks (Wang and Nowack, 2018; Piechulek et al., 2019).

The representative pollutants for "old versus emerging" pollutants iHg and nanosilica are both neurotoxic/neurodegenerative and have the potential to induce amyloid protein aggregation in human cells and *C. elegans* (Arnhold et al., 2015; Scharf et al., 2016). As it is well established that widespread protein aggregation is a hallmark of aging (David et al., 2010; Hipp et al., 2019), the proteostasis network represents a possible candidate pathway in which to test the effects of pollutants on aging. Proteostasis shapes the proteome through ribosome-associated quality control, chaperone-mediated folding, transporters, and degradation processes via proteasome, lysosomes, and autophagy. Furthermore, proteostasis mechanisms can be modulated by genetic intervention to increase health- and lifespan (Morimoto, 2020).

Here, we demonstrate that the pollutants nanosilica and iHg induce aging phenotypes by corrupting resilience pathways that normally preserve protein homeostasis and drive longevity. We show that the tested pollutants not only significantly reduce the lifespan of wild-type *C. elegans*, but also that silica NPs reverse the genetic lifespan resilience effects of *daf-2* mutants. iHg induced proteotoxic stress and characteristics of the aggregome network including components of protein folding, proteolysis, and stress response pathways. By comparative mass spectrometry of age- and pollutant-induced aggregomes, we identified a shared aggregation phenotype with enrichment for proteins involved in protein homeostasis independent of protein abundance. Furthermore, we identified nine super-aggregation proteins with links to human diseases that became insoluble and components of an aggregome during intrinsic- as well as pollutant-induced aging. These results demonstrate that pollutants negatively affect well-described aging prevention pathways and that effective pollution control and reduction will be an important strategy to fight aging and premature death worldwide.

RESULTS

Silica nanoparticles and inorganic mercury reduce lifespan

To characterize the impact of pollutants on resilience pathways of aging, we analyzed how two widely distributed pollutants, iHg and 50 nm silica nanoparticles (NPs) (von Mikecz, 2018) affect the lifespan of *C. elegans*. To determine lifespan changes, *C. elegans* hermaphrodites were treated with different concentrations of silica NPs or iHg from the L4/young adult stage in S-Medium with *E. coli* and 5-fluorodeoxyuridine (FUdR) at 20°C (Figure 1 and Table S1). We chose effective nanosilica (1.25 mg/mL) and iHg (10-50 μM) concentrations for chronic exposure according to previous studies (Arnhold et al., 2015; Piechulek et al., 2019; Scharf et al., 2013, 2016). Importantly, the chosen pollutant concentrations are environmentally relevant (Arnhold et al., 2015; Piechulek et al., 2019). For example, median nanosilica release concentrations are predicted to reach up to 270 μg/kg in natural and urban soil, 350 mg/kg in sludge-treated soil, and 1200 mg/kg in landfill waste in Europe in one year (Piechulek et al., 2019; Wang
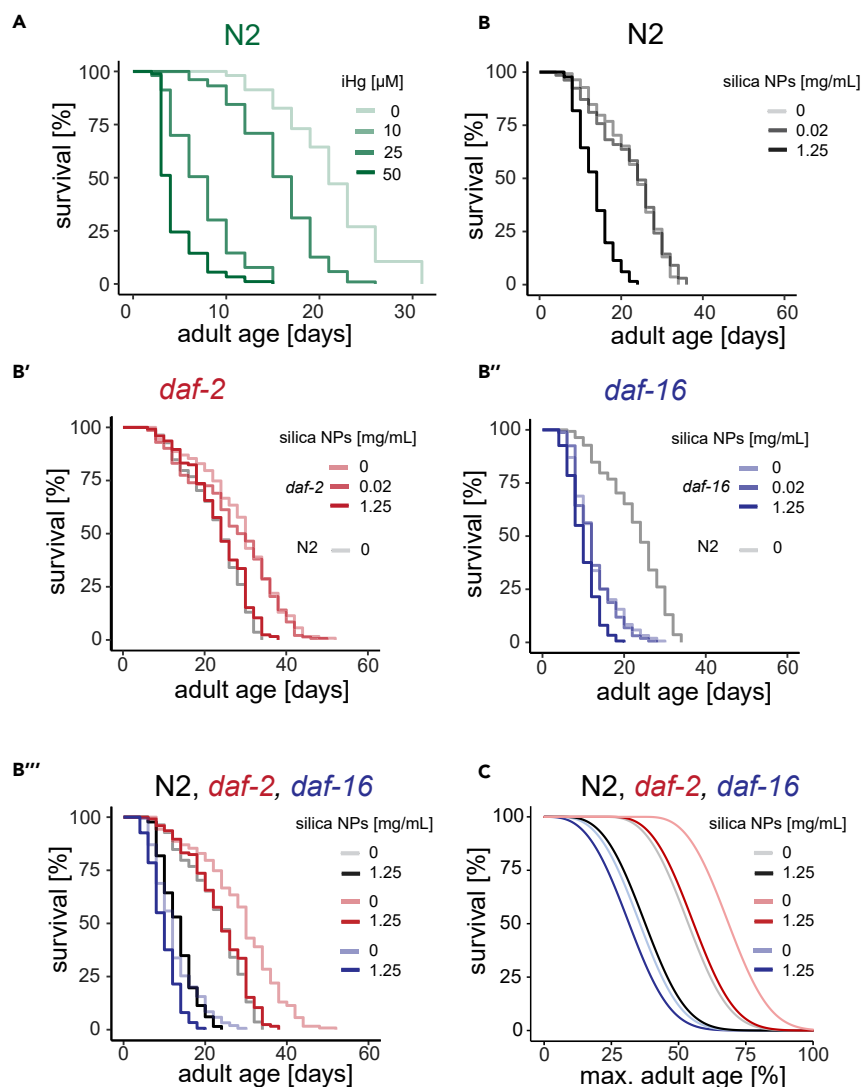
Figure 1. Environmental stressors rescale *C. elegans* lifespans

(A–C) Animals were cultured in S-medium with OP50 as a food source and supplemented with FUdR to prevent larval hatching. (A) Representative survival curves for wild-type N2 exposed to iHg from adult day 1 as indicated. See Table S1 for summary statistics. (B-C) Representative survival curves for (B) wild-type (N2), (B′) *daf-2(e1368)*, and (B″) *daf-16(mu86)* exposed to silica NPs from adult day 1 as indicated. Note that that all survival curves are from one experiment (Figure S2) and shown first separately for better visualization. N2 control is the same in B, B′, B″, and B‴. See Table S1 for summary statistics.

(B‴) Representative survival curves for wild-type N2, *daf-2(e1368)*, *daf-16(mu86)* from B, B′, and B″ exposed to silica NPs from adult day 1 as indicated. See Table S1 for summary statistics. (C) The blue, grayscale, and red (Weibull) lines represent maximum-likelihood estimation (MLE) fits of the parametric model using data up to median survival.

and Nowack, 2018). These predicted release concentrations are most likely exceeded locally owing to accidental spills or overuse of environmental pollutant and in organismal tissue owing to accumulations along the food chain as observed for mercury (Arnhold et al., 2015, Table 1). In addition, the increasing applications of nanomaterial and mercury will dramatically increase their accumulation in the environment in the future as we can observe with microplastics. To determine *C. elegans'* lifespans after exposure to iHg and nanosilica, we chose a liquid medium-based assay because it is an excellent tool for drug/pollutant delivery to *C. elegans* (Petrascheck et al., 2007), whereas FUdR diminishes the hatching of progeny including internal hatches or the so-called "bag of worms"-phenotype that is highly frequent in *C. elegans* exposed to silica NPs (Scharf et al., 2016) and iHg (Figure S1). Exposure to iHg decreased lifespans in a

Table 1. Super Aggregators are identified in the iHg-, silica NPs-, and age-specific aggregome

gene name[a]	protein[b]	GO biological process[c]	cellular localisation[d]	(Reis-Rodrigues et al., 2012)[e]	(David et al., 2010)[f]	rank abundant protein[g]	fold expression day12/day1[h]	human homolog[i]	human disease[j]
art-1	Probable very-long-chain enoyl-CoA reductase	metabolic processes	ER	–	–	355	−0.5	TECR (trans-2,3-enoyl-CoA reductase)	Autosomal Recessive Non-syndromic Intellectual Disability and Catecholaminergic Polymorphic Ventricular Tachycardia 3
dim-1	Disorganized muscle protein 1	muscle	cyto	–	4.1 fold	201	0.5	MYPN (myopalladin)	Dilated Cardiomyopathy and Nemaline Myopathy 11, Myopathy
F37C4.5	ND	ND	ND	–	3.1 fold	151	2.7		
fib-1	rRNA 2′-O-methyltransferase fibrillarin	translation, rRNA metabolic process	nu	–	3.6 fold	231	−0.5	FBL (fibrillarin)	Systemic sclerosis, Skleroderma, Myositis, Myopathy, Connective Tissue Disease, Dyskeratosis Congenita, Spinal Muscular Atrophy, Telangiectasis, Retinitis Pigmentosa
hsp-6	Heat shock protein	protein folding, proteolysis, stress response	mito	yes, yes	7.4 fold	204	−0.1	HSPA9 (heat shock protein family A (Hsp70) member 9)	Autosomal Dominant Sideroblastic Anemia 4, Even-Plus Syndrome, Parkinson Disease, Late-Onset, 1 Friedreich Ataxia, Codas Syndrome, Myositis Ossificans, Alternating Esotropia
lec-1	32 kDa beta-galactoside-binding lectin	extracelluar matrix	extra	–	4.6 fold	432	0.4	LGALS9 (galectin 9); LGALS9B (galectin 9B); and LGALS9C (galectin 9C)	Cone-Rod Dystrophy 2, Systemic Lupus Erythematosus, Rheumatoid Arthritis
rpl-2	60S ribosomal protein L8	translation, rRNA metabolic process	nu, cyto	–	7.4 fold	38	−0.4	RPL8 (ribosomal protein L8)	Cystic Renal Dysplasia, Spermatogenic Failure 1&2
rpl-22	60S ribosomal protein L22	translation, rRNA metabolic process	nu, cyto	–	4.4 fold	55	−0.3	RPL22 (ribosomal protein L22)	Myelodysplastic Syndrome, Diamond-Blackfan Anemia
rpl-7	60S ribosomal protein L7	translation, rRNA metabolic process	nu, cyto	yes, yes	5.5 fold	35	−0.4	RPL7 (ribosomal protein L7)	Systemic Lupus Erythematosus, Diamond-Blackfan Anemia

ND, not determined; nu, nucleus; mito, mitochondria; ER, endoplasmatic reticulum; cyto, cytoplasm; extra, extracellular.

[a]Gene name according to WormBase (Harris et al., 2020).

[b]Protein according to PANTHER, UniProt, or WormBase database.

[c]GO biological process: classified according to PANTHER database. Additional UniProt, Wormbase, and Literature mining.

[d]Cellular Localisation accoding PANTHER, UniProt, or WormBase database.

[e]Candidate of age-specific aggregome identified, lifespan prolonged if mutated/knockdown via RNAi (Reis-Rodrigues et al., 2012).

[f]Candidate of age-specific aggregome identified in (David et al., 2010).

[g]All proteins characterized in Walther et al. (2015) were ranked according their abundance on day 12.

[h]Relative abundance values of proteins on day 12 compared to day 1 (Walther et al., 2015).

[i]Human homologs according to WormBase.

[j]Human diseases according to WormBase and https://www.malacards.org/.

concentration-dependent manner with 10, 25, and 50 μM iHg reducing mean lifespans by 14%, 61%, and 80%, respectively (Figure 1A and Table S1). Maximum lifespans after iHg exposure were decreased by 8%, 55%, and 61%, respectively (Figure 1A and Table S1). Although low concentrations of silica NPs did not show any significant changes in lifespan, 1.25 mg/mL of silica NPs decreased the mean and maximum lifespan by 36% and 25% respectively (Figure 1B and Table S1).

Silica nanoparticles interfere with genetic lifespan resilience effects

Next, we investigated whether aging interventions protect against the lifespan-shortening effects of silica NPs using *C. elegans* strains carrying mutations in the IGF signaling pathway (Figures 1B and 1C and S2 and Table S1). Mutations in the *daf-2*/insulin/IGF-1-receptor gene extend lifespan via activation of the DAF-16/FOXO transcription factor-mediated protection gene program, whereas *daf-16(lf)* strains show reduced lifespans compared to wild-type strains (Kenyon et al., 1993). We chose this genetic intervention owing to its effective lifespan extension phenotype and potential to prevent protein aggregation (David et al., 2010), as silica NPs induce protein aggregation in young *C. elegans* (Scharf et al., 2013). We further chose a *daf-2* mutant strain with the e1368 allele in contrast to the often used e1370 allele, because mutants with the e1368 allele exhibit less developmental defects (Gems et al., 1998). Silica NP treatment significantly decreased the mean and maximum lifespan of *daf-2(e1368)* mutant animals by 15% and 24% (Figures 1B′ and B‴ and Table S1). Similarly, *daf-16(mu86)* loss-of-function mutant animals (Lin et al., 1997) exhibited a 25% shorter mean and a 31% shorter maximum lifespan when treated with silica NPs (Figures 1B″ and B‴ and Table S1). We can exclude that the observed lifespan effects are owing to reduced viability of silica NPs exposed to *E. coli* (Figure S3); however, it is still possible that pollutants affect bacteria without changing the viability and induce secondary effects. It is also possible that the usage of FUdR could have affected the conducted lifespan experiments by increasing the lifespans or interacting with the pollutants. However, in the case of a potential FUdR-induced lifespan extension, we still can conclude that silica NPs shorten the lifespan of all exposed strains. In conclusion, silica NPs diminished any effect of the positive genetic intervention on prolonging the lifespan.

To investigate whether pollutants activate the DAF-16-dependent stress response, we analyzed DAF-16 localization in intestinal cells using a transgenic strain with an integrated DAF-16::GFP (Henderson and Johnson, 2001). Many stressors, such as heat, UV, or oxidative stress, induce DAF-16 translocation into the nucleus to activate a stress-protection and longevity gene program (Lin et al., 2018). *C. elegans* exposed to 0.1 and 1.25 mg/mL silica NPs or 25 and 50 μM iHg exhibit a significant increase in animals with nuclear DAF-16 accumulation (Figure 2). These results support the conclusion that silica NPs and iHg activate a classic stress response pathway; however, the activation of the DAF-16-dependent gene program does not protect the animals against the lifespan-shortening effect of silica NPs and iHg.

Silica nanoparticles and inorganic mercury induce proteotoxic stress

Temporal scaling of lifespan distributions is a feature of most aging interventions that are based on a shared organismal state also called resilience or vitality (Stroustrup et al., 2016). Therefore, if pollutants are negative aging interventions, they will also affect aging by influencing the same organismal state or resilience pathway. Consistent with this, exposure to silica NPs shifted the lifespan distribution of *daf-2(lf)* mutants back to wild-type and of wild-type animals back to *daf-16(lf)* mutants (Figures 1B‴ and C and Table S1).

Proteostasis is a possible candidate for such a resilience pathway given that (1) the disruption of proteostasis is a hallmark of intrinsic aging that manifests as the accumulation of protein aggregates (Hipp et al., 2019), and (2) several studies have shown that pollutants and xenobiotics can induce protein fibrillation and disrupt proteostasis (Arnhold et al., 2015; Chen et al., 2008). Furthermore, xenobiotic exposure can be linked to neurodegenerative diseases such as Parkinson's or Alzheimer's disease and can induce pathogenic protein aggregation of amyloid-like assemblies containing several hundred proteins as well as non-proteinaceous components including metals (Gerhardsson et al., 2008; Lashuel, 2021; Meleleo et al., 2020; Uversky et al., 2001).

We predicted that if proteostasis is the underlying resilience pathway, silica NPs and iHg-exposed *C. elegans* would share features of the protein aggregation phenotype with aged *C. elegans*. To investigate this, we first used a transgenic *C. elegans* model for proteotoxic stress in muscle cells that allows the visualization of age-related induction of polyglutamine (polyQ) fibrillation (Morley et al., 2002). This strain expresses
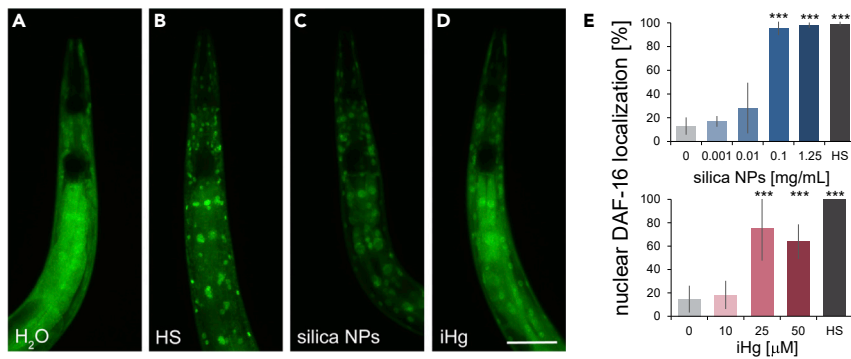
Figure 2. Environmental stressors activate DAF-16-dependent stress response

(A–D) Representative fluorescent micrographs of 2-day-old, adult *C. elegans* expressing DAF-16 fused to green fluorescent protein (DAF-16::GFP) in the anterior-most intestinal cells (Henderson and Johnson, 2001). Scale bar: 100 μm

(A) DAF-16 is globally expressed in mock (H_2O)-treated hermaphrodites and translocates to the nucleus under (B) heat stress (15 min. at 37°C) and after the exposure to (C) silica NPs or (D) inorganic mercury after 24 h.

(E) Nuclear translocation of DAF-16 was scored and compared to control. Values represent +/- SD of 4-5 independent experiments with n = 20-33 per treatment per experiment (one-way ANOVA with Tukey's post-hoc test). ***$p < 0.001$; HS, heat stress.

homopolymeric repeats of 35 glutamines fused to yellow fluorescent protein (Q35::YFP) in muscle cells of the body wall. Young Q35::YFP *C. elegans* showed a smooth fluorescent pattern along the muscle fibers which changes in an irregularly dotted pattern of polyQ aggregates with age (Morley et al., 2002). We showed previously that silica NPs induce polyQ aggregation in younger animals (Table S2) (see Figures 1B and 1C in Scharf et al., 2016 https://doi.org/10.3109/17435390.2015.1073399). To analyze whether iHg induces a similar phenotype, we exposed Q35 animals on adult day 1 to 60 μM iHg or left them untreated (H_2O) for 24 h. Untreated Q35 *C. elegans* showed a mostly smooth distribution of yellow fluorescence along the body wall muscles on adult day 2 (Figures 3A and 3B and S4), consistent with previously published observations (Morley et al., 2002). Similar to silica NPs, exposure to iHg prematurely induced the dotted pattern of aggregated polyQ typical for animals older than adult day 3 (Figures 3A and 3B and S4). Quantification of the fluorescent polyQ aggregates showed a significant 1.9-fold increase in the number of aggregates after iHg exposure. This result indicates that iHg induces proteotoxic stress in young *C. elegans*, which is supported by the previous observations that iHg induces the fibrillation of endogenous proteins in the nucleolus of intestinal cells in *C. elegans* as well as causes the aggregation of nuclear proteins in human cells (Table S2). Notably, silica NPs induced the same age-related aggregation phenotype as we showed in a previous study (Table S2) (Scharf et al., 2016). In summary, the two candidate pollutants iHg and silica NPs induce widespread protein aggregation in young *C. elegans* that manifests on the local and global level representing a premature aggregation phenotype that normally develops during the intrinsic aging process.

Inorganic mercury-induced aggregome network

Previously, we identified the components of the silica NP-induced aggregome network in *C. elegans* via filter retardation assay and mass spectrometry (Scharf et al., 2016). An aggregome network describes proteins that sequester into amyloid-like protein aggregates inside cells or whole organisms. To compare the silica NP- and iHg-induced aggregome networks, we now also characterize the iHg-induced aggregome network. Wild-type day 1 adults were either left untreated (H_2O) or exposed to 50 μM iHg for 24 h, lysed, and the SDS-insoluble protein fraction isolated via filter retardation assay (Scheme, Figure S5) (Scherzinger et al., 1997). This method specifically traps SDS-insoluble high molecular weight protein aggregates, also referred to as amyloid-like protein aggregates. The soluble fraction, including less stable amorphous protein aggregates, passes through the 0.2 μm pores of cellulose acetate membranes, whereas the amyloid-like proteins are trapped (Wanker et al., 1999). In order to identify the amyloid-like proteins, we eluted and analyzed the trapped SDS-insoluble protein fraction via mass spectrometry, gene ontology (GO) analysis, and data mining. We identified 89 proteins that aggregated specifically in iHg-exposed *C. elegans*, whereas 59 proteins aggregated independently of iHg exposure (Figure 3C and Table S3). We defined these two groups of SDS-insoluble proteins as mercury-specific aggregome and as ground state
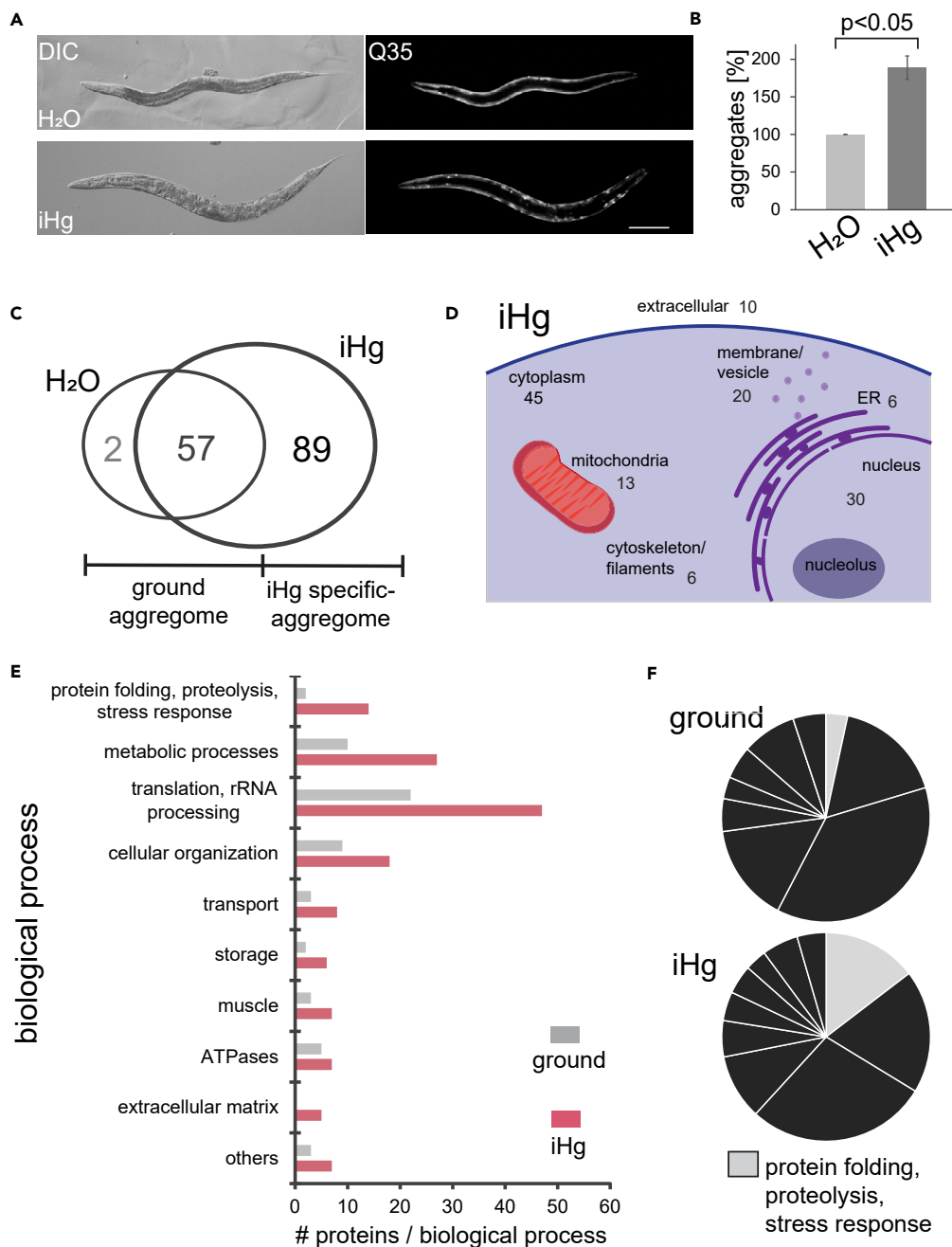
Figure 3. Inorganic mercury accelerates protein fibrillation in adult *C. elegans*

(A) Representative fluorescent micrographs of 2-day-old, adult hermaphrodites of a *C. elegans* proteotoxic stress model that expresses homopolymeric repeats of 35 glutamines fused to yellow fluorescent protein (Q35::YFP) in body wall muscle cells (Morley et al., 2002). Hermaphrodites were mock-treated or exposed to 60 μM iHg for 24 h. Bar, 100 μm. Note that the same hermaphordites were shown in comparison to 1, 3, and 4 days old untreated and iHg exposed worms in Figure S4. All images show whole *C. elegans* cut out of larger images.

(B) Respective quantification of the increase in Q35-YFP aggregates per hermaphrodite compared to control. Values represent +/- SD of three independent experiments with n ≥ 90 for each treatment. Student's *t* test $p < 0.05$ for H₂O versus iHg. Compare these results to Figures 1B and 1C in Scharf et al. (2016), https://doi.org/10.3109/17435390.2015.1073399.

(C) Venn-diagram of the insoluble protein fraction of 24-h mock-treated or iHg-exposed wild-type *C. elegans*. We defined proteins that aggregate specifically in iHg-exposed *C. elegans* as iHg-specific aggregome and all other SDS-insoluble proteins as ground state aggregome respectively.

Figure 3. *Continued*

(D) Cellular localization of iHg-specific insoluble proteins. The numbers indicate the number of identified candidate proteins associated with each cellular subcellular compartment according to data mining of the PANTHER database (Mi et al., 2013), UniProt (UniProt Consortium, 2021) , and WormBase (Harris et al., 2020). Note that a candidate protein can be in more than one subcellular compartment.

(E) GO analysis of the ground and complete iHg-induced aggregome. Each identified insoluble protein was categorized according to its biological process classified using the PANTHER database, UniProt, WormBase, and literature. The graph presents the absolute number of identified SDS-insoluble proteins per biological process category.

(F) The functional group protein folding, proteolysis, and stress response show the highest increase in insoluble proteins in iHg-exposed *C. elegans* as illustrated in the pie chart.

aggregome, respectively. Although proteins of the iHg-specific aggregome localized throughout the cell, proteins were mostly associated with the cytoplasm, nucleus, and membranes (Figure 3D). Interestingly, the nucleus is the organelle with the largest fraction of different insoluble proteins in the ground state and after iHg exposure. The insoluble fraction included many ribosomal proteins, but also prominent nucleolar proteins such as fibrillarin (FIB-1) (Table S3). GO analysis revealed that the iHg-induced aggregome network is enriched with proteins related to the biological functions of "metabolic processes" (17 out of 89 proteins) and "translation and RNA processing" (25 out of 89 proteins) (Figure 3E and Table S3). Furthermore, proteins with the biological function of "proteolysis and stress response" showed the largest increase after iHg exposure (Figures 3E and 3F). The two functional groups "translation and RNA processing" and "proteolysis and stress response" can be combined as functional group "proteostasis," accounting for over 43% of proteins identified in the iHg-specific aggregome.

Comparison with the previously described silica NP-induced aggregome network (Scharf et al., 2016) revealed 19 shared proteins that fibrillate after exposure to iHg and silica NPs (Figure 6). In addition, both aggregome networks showed the largest enrichment of proteins with the biological functions "metabolic processes," "translation and RNA processing," and "proteolysis and stress response." Therefore, proteins that drive protein homeostasis ("translation and RNA processing" and "proteolysis and stress response" combined) showed the largest increase after exposure to silica NPs and iHg. Specifically, the chaperones HSP-6 and HSP-60 as well as the proteasome subunits RPN-2 and RPN-3 were shared components of both aggregomes. These proteins are essential for maintaining proteostasis and likely sequester to microenvironments in the cell to dissolve protein aggregations. In addition, many proteins that are essential for the first steps of proteostasis such as protein translation were also part of the aggregomes. Although chaperones and proteasomes may be functional components of the amyloid-like protein aggregates (Chen et al., 2008), proteins necessary for protein synthesis are most likely dysfunctional in their amyloid-like protein state. Consequently, fine-tuned cellular and organismal proteostasis are disturbed. This result supports the hypothesis of proteostasis as a central resilience pathway controlling lifespan and aging.

Age-induced aggregome-network

Next, we asked whether iHg and silica NPs (1) induce the aggregation of proteins in young animals that normally aggregate with old age or (2) induce the insolubility of a specific set of proteins that are different from the age-induced aggregome. In order to answer this question, we analyzed age-induced insoluble protein data sets from the literature. The Kenyon lab identified 461 proteins with an age-dependent shift to an insoluble state using two temperature-sensitive sterile strains: the gonad-less mutant *gon-2* and the germline-deficient mutant *glp-1* at 25°C (David et al., 2010). The Lithgow and Hughes labs identified 203 proteins that shift age-dependently to an insoluble state by using the temperature-sensitive sterile strain TJ1060 (*spe-9(hc88)I*; *fer-15(b26)II*) (Reis-Rodrigues et al., 2012). These two datasets shared 118 proteins that became insoluble in aged *C. elegans* (Figure 4E and Tables S4 and S5). Both approaches used centrifugation-based separation of the insoluble and soluble protein fractions with SDS-containing buffers and resuspension with 70% formic acid. We reasoned that by using the amyloid-specific filter trap assay (Scherzinger et al., 1997) to analyze the aged aggregome network in wild-type *C. elegans*, we would add a dataset containing proteins that form age-dependent amyloid-like aggregates. Therefore, wild-type (N2) *C. elegans* were cultured on agar plates supplemented with FUdR to prevent egg hatching and lysed at adult day 1 (young) and adult day 12 (old). The SDS-insoluble protein fractions were isolated via filter retardation assay (Figure S5, (Scherzinger et al., 1997)) and analyzed by mass spectrometry. We identified 78 proteins that aggregate specifically with old age, whereas 31 proteins are already insoluble in young animals (Figure 4A and Table S6). We defined these two groups as old age-specific aggregome and ground aggregome respectively. Over 65% of the identified proteins of the old age-specific aggregome were enriched
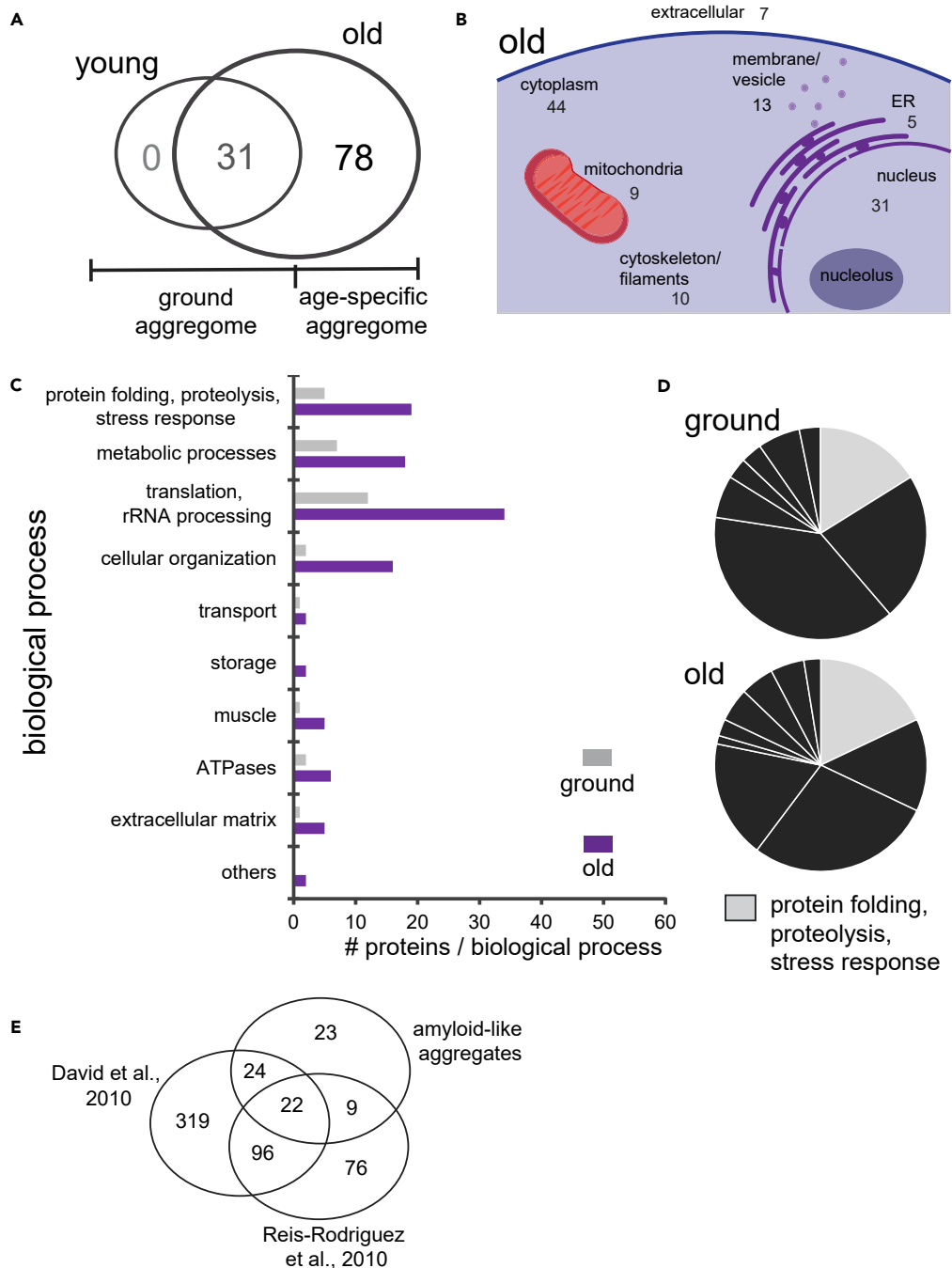
Figure 4. Age-related amyloid protein fibrillation in *C. elegans*

(A) Venn-diagram of the insoluble protein fraction of 1- (young) and 12-day (old) adult wild-type *C. elegans*. We defined proteins that aggregate specifically in 12-day-old adult *C. elegans* as age-specific aggregome and all other SDS-insoluble proteins as ground state aggregome respectively.

(B) Cellular localization of age-specific insoluble proteins. The numbers indicate the number of identified candidate proteins associated with each cellular subcellular compartment according to data mining of the PANTHER database (Mi et al., 2013), UniProt (UniProt Consortium, 2021), and WormBase (Harris et al., 2020). Note that a candidate protein can be in more than one subcellular compartment.

(C) GO analysis of the ground and complete age-induced aggregome. Each identified insoluble protein was categorized according to its biological process classified using the PANTHER database, UniProt, WormBase, and literature. The graph presents the absolute number of identified SDS-insoluble proteins per biological process category.

Figure 4. *Continued*

(D) The change in the functional group protein folding, proteolysis, and stress response in young versus old *C. elegans* is illustrated in the pie chart.

(E) Comparative mass spectrometry based on different biochemical preparations: Venn diagram of insoluble proteins identified in David et al. (2010) and Reis-Rodrigues et al. (2012) compared to the amyloid-like protein aggregates identified in this study.

in the insoluble protein fractions reported in the David et al. (2010) and Reis-Rodrigues et al. (2012) datasets. All three data sets shared 22-old-age-induced insoluble proteins, seven of which play a role in proteostasis (Figure 4E and Tables S4 and S5). Thus, comparative mass spectrometry based on different biochemical preparations clearly provides an added value by further clarification of the cellular pathways. Here, the comparative dissection of age-induced protein aggregates reveals proteostasis as a specific pathway of amyloid formation.

Pollutant- and old age-induced aggregation phenotype

Next, we compared the old age-induced aggregome with the iHg- and silica NPs-induced aggregome networks. Proteins aggregate throughout the cell after iHg exposure and in old *C. elegans*. In agreement with the iHg-specific aggregome, the cytoplasm, nucleus, and membranes of the age-induced aggregome network showed the highest amount of age-induced insoluble proteins (Figure 4B). GO-analysis revealed that the old age-induced aggregome network was also enriched for proteins related to the biological functions of "proteolysis and stress response," "metabolic processes," and "translation and RNA processing" (Figure 4C). In contrast to the iHg- and silica NP-induced aggregome networks, proteins with the biological functions of "cellular organization" showed the largest increase of proteins in the SDS-insoluble amyloid-like protein fraction in old *C. elegans* compared to the ground state. Although structural proteins such as the intermediate filament IFB-2 (human ortholog lamin B2) or IFC-2 (human orthologs include keratin 72,74,83) are not affected by xenobiotic-induced premature aging, they are an intrinsic part of the old age-induced aggregome network.

One possible explanation is that these structural proteins aggregate because of the age-related reduced capacity of chaperones and clearance machinery. The decline of the proteostasis network owing to reduced expression (Ben-Zvi et al., 2009) and increased sequestration of its components to protein aggregates with age causes an increasing solubility imbalance in the organism highlighted by the insolubility of structural proteins in the aged-induced aggregome. In agreement, IFB-2 was identified as one of the 10 age-dysregulated proteasomal targets, which mislocalizes into cytosolic protein aggregates linked to loss of intestinal integrity (Koyuncu et al., 2021). Furthermore, knockdown of *ifb-2* in adult *C. elegans* results in an increased lifespan and better intestinal health (Koyuncu et al., 2021). Future studies that include longitudinal experiments could time stamp the appearance of different functional protein groups in the insoluble fraction and allow the construction of an insolubility timeline.

We also compared the structural features of the proteins in old age-, iHg-, and silica NP-induced aggregome networks (Figure 5). All three aggregome networks were enriched with proteins containing beta strands, cross-links, helices, nucleotide binding capacities, and repeats. Only a few features were specific for a single aggregome. The xenobiotic-induced aggregomes exhibited an overrepresentation of zinc finger-containing proteins. Proteins with metal binding domains were only enriched in the iHg-induced aggregome, whereas the old age-induced aggregome showed not even one zinc finger protein.

Overall, all three aggregome networks showed many similarities including protein features and functional groups. Proteins that drive the protein homeostasis were the most enriched proteins in the old age-, iHg-, and silica NP-induced aggregome networks (Tables S3 and S6 and Figures 3 and 4 and S6 and S7 (Scharf et al., 2016). This result supports the hypothesis that proteostasis represents a central resilience pathway, controlling lifespan. We showed that *C. elegans* exposed to iHg- and silica NPs induce an aggregome network, which resembles many features of aggregome networks of old animals. This is consistent with the idea that pollutants impair the physiology of animals by corrupting the respective resilience pathways of intrinsic aging.

Identification of super aggregation proteins

Given that the two pollutants studied, iHg and nanosilica, induce protein aggregation phenotypes that share many characteristics with aggregation phenotypes observed during intrinsic aging, we would expect
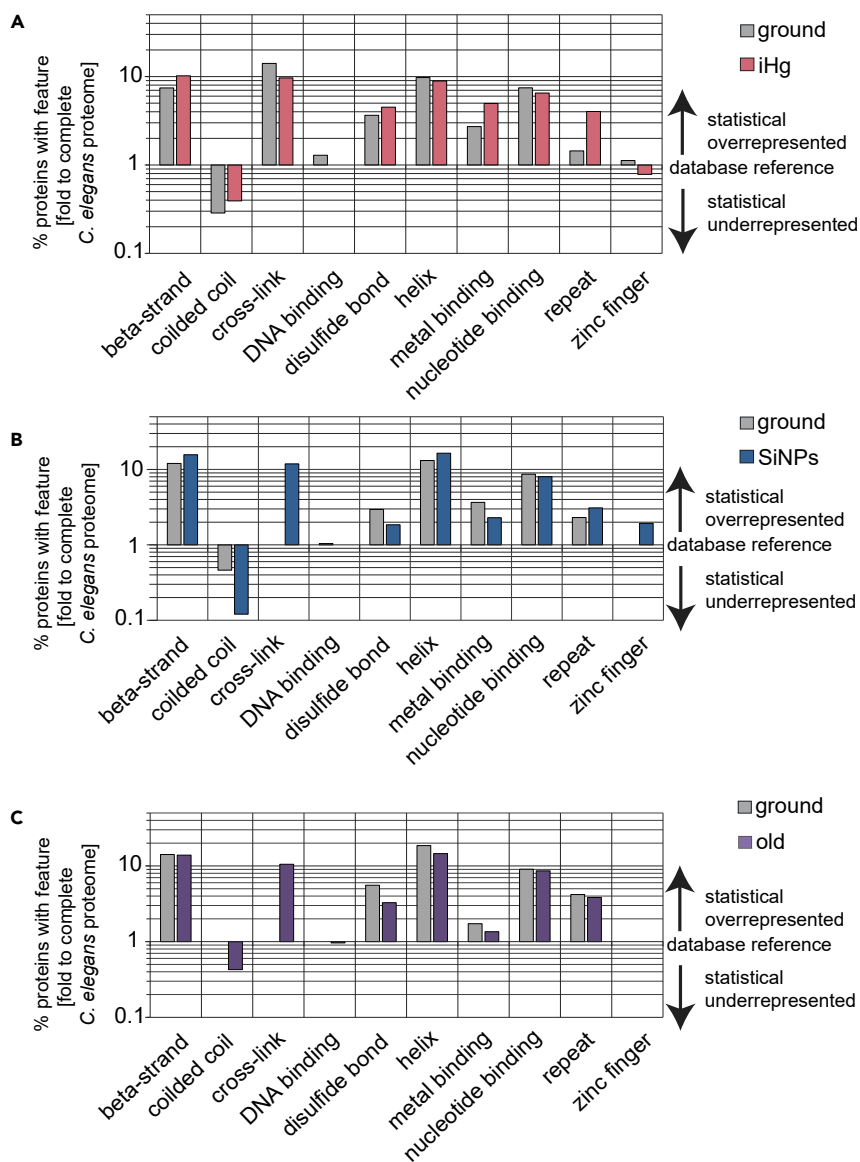
Figure 5. Shared structural protein feature of aggregome networks
Analysis of structural protein features of the (A) iHg-, (B) silica NPs- (Scharf et al., 2016), and (C) age-induced aggregomes based on the UniProt database (UniProt Consortium, 2021). The identified fibrillated proteins show a statistical overrepresentation in beta strands, cross-links, helices, and nucleotide binding. Metal binding is only overrepresented in the iHG-induced aggregome, and zinc fingers are absent from the age-induced aggregome.

that the same proteins segregate into the aggregome networks. Consistent with this, we found nine super aggregation proteins that were present in the iHg-, silica NP-, and age-induced aggregome networks (Figure 6 and Table 1), suggesting that the three aggregome networks are more than 10% identical. The silica NP- and iHg-aggregome networks shared 10 proteins, whereas 14 were shared between the iHg-induced and old aggregome network and 12 proteins were shared between the silica NP-induced and the old aggregome network.

An alternative explanation for the identification of proteins with similar functions and even shared proteins in all three aggregomes could be their abundance in the tissues of *C. elegans*. To exclude that the identified proteins are just the highest expressed proteins under the different conditions, we first mined the mass spectrometry dataset from Walther et al. (2015) for changes in abundance levels of proteins in old
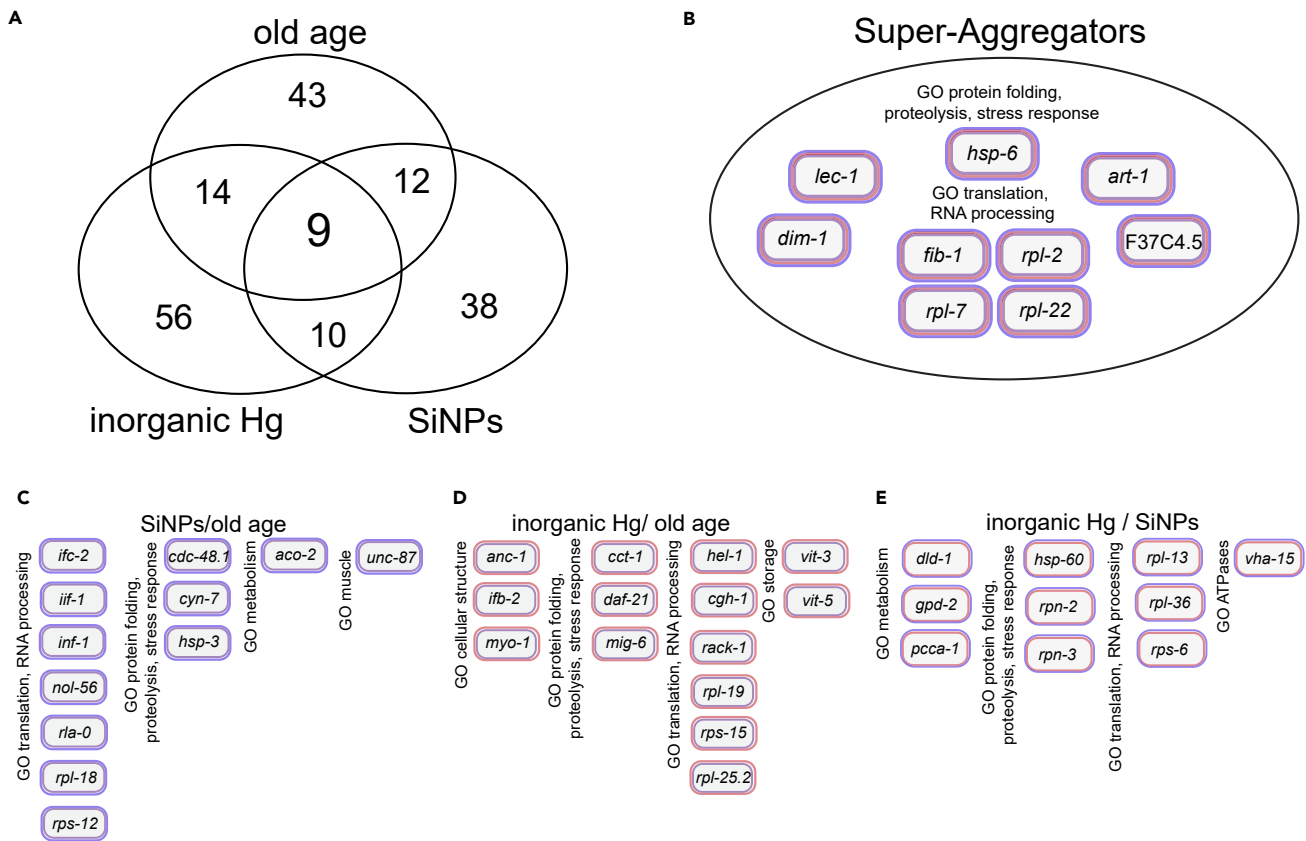
Figure 6. Identification of 9 super aggregators shared between aggregomes

(A) Venn diagram of insoluble proteins of the iHg-, silica NPs- (Scharf et al., 2016), and the age-induced aggregome.

(B) All three aggregomes share 9 super aggregator proteins: HSP-6, FIB-1, RPL-2, RPL-7, RPL-22, ART-1, LEC-1, DIM-1, and F37C4.5. Shared identified insoluble proteins between only (C) the silica NPs- and the age-induced aggregome, (D) iHg- and the age-induced aggregome, and (E) between the iHg- and silica NPs-induced aggregome.

compared to young N2 *C. elegans* (Table 1). AHCY-1 was the most abundant protein in day-1 *C. elegans* in the data set (Walther et al., 2015) and was identified as insoluble protein in the ground aggregome here. In contrast, RPL-30 was the second most abundant protein in adult day 1 *C. elegans* and 28th most abundant protein in adult day 12 worms (Walther et al., 2015), but was not identified in any aggregome. All nine super aggregation proteins ranked in the first 600 out of nearly 6000 proteins with abundance data in adult day 1 and adult day 12 *C. elegans* (Table 1). Nevertheless, 7 of the 9 proteins are less abundant in 12-day old compared to 1-day-old *C. elegans* (Table 1). This trend was confirmed with qPCR for the protein FIB-1 and HSP-60. Both proteins did not show any significant change in mRNA expression after iHg-treatment, whereas HSP-6 exhibited a 11-fold induction in mRNA expression (Figure S8). Although we concluded that the identified aggregomes do not simply reflect just the most abundant proteins, it is still possible that highly abundant insoluble proteins are more likely detected than less abundant insoluble proteins.

The nine super aggregation proteins were ART-1, the probable very-long-chain enoyl-CoA reductase; HSP-6, a mitochondrial chaperone; FIB-1, the rRNA 2′-O-methyltransferase fibrillarin; DIM-1, the disorganized muscle-protein 1; LEC-1, a 32 kDa beta-galactoside-binding lectin; the unnamed protein F37C4.5; and the three ribosomal proteins RPL7/L7, RPL2/L8, and RPL22/L22 (Table 1). All these proteins, except for ART-1, were also identified in the age-induced insoluble protein fraction of two temperature sensitive sterile strains: the gonad-less mutant *gon-2* and the germline-deficient mutant *glp-1* at 25°C (David et al., 2010), which validates the significance of these super aggregation proteins in the development of aggregome networks. Furthermore, all proteins, except for F37C4.5 (homologs are not identified yet), have homologs in humans that are linked to human diseases (Table 1). Most of these super aggregators are protein homeostasis proteins, which supports the hypothesis of proteostasis as a central resilience pathway controlling aging and lifespan.
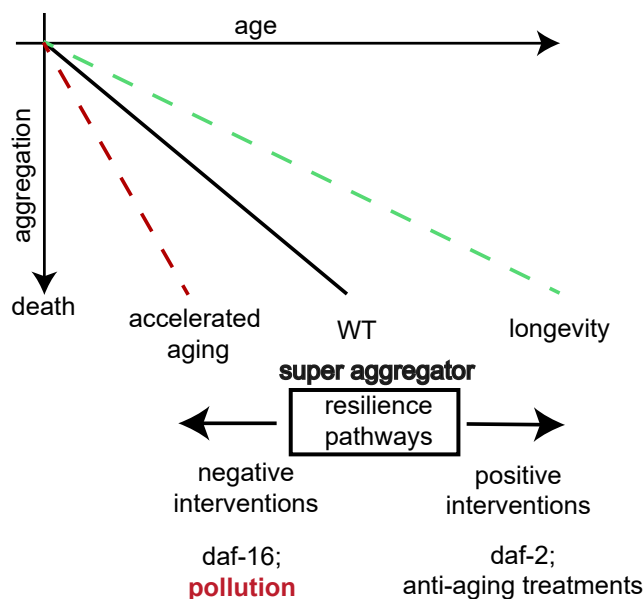
Figure 7. Pollutants hijack resilience pathways of intrinsic aging
The schematic shows how negative interventions and positive interventions change the fibrillation status of an organism and affect its aging rate. We propose that genetic interventions such as *daf-16* and *daf-2* loss of function mutations, anti-aging treatments such as HSP-90 inhibitors, or pollution such as the well-known pollutant iHg as well as the emerging pollutant silica NP affect the same resilience pathways that normally preserve cellular homeostasis and thereby modify aging processes. In conclusion, reducing pollution and controlling the synthesis of new compounds have to be an important part of an effective strategy to support healthy aging.

Possible effects of the aggregation of proteostasis proteins

Interestingly, experiments with HSP-6 and RPL-7, two proteostasis proteins, showed opposite effects on *C. elegans* lifespan in previous studies: reduction of *hsp-6* reduces lifespan (Kimura et al., 2007), whereas the reduction of *rpl-7* increased the lifespan (Reis-Rodrigues et al., 2012). The functions of these two proteins can explain the different effects on lifespan. RPL-7 is a ribosomal protein that localizes in the nucleolus during ribosomal RNP subunit assembly and in the cytoplasm as part of ribosomes. Although RPL-7 is normally abundant in the cell, it shows a 0.4-fold decreased relative abundance in the proteome of old worms compared to young worms (Table 1) (Walther et al., 2015). Consequently, the appearance of RPL-7 as a super aggregation protein in induced aggregome networks is not just caused by abundance. Ribosomal proteins are aggregation-prone owing to unfolded extensions and basic regions that are essential for their interactions with rRNAs (Pillet et al., 2017). It seems likely that such a protein will fibrillate and drive protein aggregation once the proteostasis is misbalanced owing to aging or pollutant stressors. Knockdown of *rpl-7* reduces the burden of insoluble proteins and crowding effects in the nucleus/nucleolus (Vecchi et al., 2020), which results in an increased lifespan. In contrast to RPL-7, HSP-6 is the mitochondrial HSP-70, highly conserved, and can prevent aggregation (Bender et al., 2011). The protein is prone to self-aggregation with the important feature that aggregated mHSP70 preserves its chaperone function (Kiraly et al., 2020). Nevertheless, it seems likely that HSP-6 and other chaperones become part of the aggregome networks by binding to increasing amounts of misfolded and fibrillated proteins. Owing to their sequestration into protein aggregation, these chaperones are unavailable for their physiological clients to assist them during folding and sustaining a healthy proteome, a process called chaperone competition (Yu et al., 2019), creating a vicious cycle (Ben-Zvi et al., 2009; Santra et al., 2019). Consequently, the organism experiences widespread protein aggregation, protein dysfunction, and failure of organs and tissues with age (Santra et al., 2019), which can be accelerated through pollutant exposure.

DISCUSSION

The concept of environmentally induced diseases and premature death (Landrigan et al., 2018) is supported by the animal model *C. elegans*. Here, we show that the well-known xenobiotic iHg and the emerging pollutant nanosilica corrupt the same resilience pathways that normally preserve cellular

homeostasis and thereby induce phenotypes in young animals that are typical for much older animals (Figure 7 and Table S2). Silica NPs accelerate global protein aggregation (Scharf et al., 2013) and reverse the genetic activation of resilience pathways through loss of function mutations in the *daf-2* gene. The capacity of the proteostasis network to resolve misfolded and damaged proteins declines in early adulthood in *C. elegans* (Ben-Zvi et al., 2009) and causes an age-related increase in protein aggregation manifested in an old age aggregation phenotype. The decline of the proteostasis network is most likely temporally fine-tuned to secure reproduction which peaks on day 2/3 of adulthood under normal condition (Scharf et al., 2021). This conclusion is supported by the observation, that most somatic age-related changes occur after the decline of reproduction (Pickett et al., 2013) . Exposure to pollutants such as iHg and nanosilica adds additional proteotoxic stress to the declining proteostasis network. As a result, the fine-tuned resilience pathway reaches the tipping-point earlier resulting in global aggregation phenotypes, accelerated somatic decline (Piechulek et al., 2019; Scharf et al., 2013), and death of the animal.

The identified fibrillated proteins can be categorized into four different groups: (1) functional amyloid, (2) highly unstructured and "sticky"/aggregation-prone proteins, (3) components of the proteostasis network, and (4) "victims" of failed proteome maintenance. (1) Functional amyloid proteins can form fibrillar aggregates as part of their executive function. For example, many RNA/DNA interacting proteins contain polyQ repeats that support the dynamic interaction at promoters during gene expression (von Mikecz, 2014). These proteins are sensitive to the crowding status of the cellular environments, and overcrowding can easily shift the balance to dysfunctional fibrillation. Proteins such as FIB-1 and many ribosomal proteins fit into this category. (2) By contrast, many of the identified proteins exhibit unstructured regions or protein features that are aggregation-prone and result in pathological fibrillation in the absence of a functional proteostasis network. Interestingly, HSP-6 and proteasome subunits belong in this category. (3) Components of the proteostasis network such as chaperones or the proteasome bind to fibrillated proteins in order to restore functional folding, therefore, sequestration to local protein aggregation environments is part of their function. (4) Finally, "victims" of failed proteome maintenance are proteins that are normally refolded and/or cleared but remain in their cellular environment owing to missing proteostasis network capacities. Proteins such as IFB-1 fall into this category and are more specifically associated with the age-induced aggregome. Proteins of all four groups constitute the amyloid protein fibrillation landscape spanning from the facilitation of functional protein interactions to pathological aggregates (von Mikecz, 2009; Lashuel, 2021). Consistent with this, deciphering the proteomes of intrinsic vs pollutant-induced aging has the potential to advance translational research in neurodegenerative diseases where age is the prominent risk factor and additional environmental factors such as traffic-related air pollution are highly suspected (Haghani et al., 2019; von Mikecz and Schikowski, 2020).

Here, we presented the intrinsic vs pollutant-induced aggregation landscape and identified super aggregation proteins in *C. elegans* exposed to two pollutants, iHg and silica NPs. Our future goal is (1) to go deeper into the role of these super aggregation proteins in pollution-induced aging as well as intrinsic aging and (2) to go broader by systematically screening pollutants for their effects on lifespan and the organismal aggregome. (1) Most of the super aggregation proteins are so essential for the development and health of the organisms that knockdowns and exposure to pollutants will be difficult to conduct and interpret with the additional stress through pollution exposure. Therefore, one future direction is to develop mutant strains via CRISPR that allow the controlled tissue-specific knock-down and overexpression of the super aggregation proteins for short periods of time. Another direction is to develop strains with mutations in the super aggregation proteins that would protect them from aggregation and/or increases their aggregation potential. (2) The vast amount of new chemicals and pollutants with unknown bio-interactions calls for an automation approach. The lifespan machine (Stroustrup et al., 2016) could allow the systematic analysis of lifespan effects of chemicals and pollutants in *C. elegans* in an automated high throughput approach. Chemicals/pollutants could then be classified according to their lifespan-shortening effects. We show that pollutants corrupt resilience pathways of intrinsic aging. As a result, pollutants negatively affect the same prevention pathways of aging that are targeted by possible anti-aging therapeutics such as HSP90 inhibitors (Janssens et al., 2019). Thus, controlling and reducing pollution is an effective strategy for aging and disease prevention.

Limitations of the study

Here we compare the aggregomes of aging *C. elegans* exposed to the pollutants mercury or nanosilica by mass spectrometry-based proteomics. This technique provides considerable volumes of data that must be analyzed. When we consider approximately 350,000 chemicals in production and use worldwide it becomes clear that with omics only a tiny subfraction of the biological response to pollutants can be

investigated. Additionally, chemicals generally act as mixtures under non-chemical environmental conditions such as changing temperatures which further multiplies to a comprehensive exposome. To cover the pollutome by omics techniques, the invertebrate *C. elegans* provides a promising model organism, but rigorous automation of liquid culture in multi-well plates and simplification of mass spectrometry, i.e. single worm proteomics, are needed for comparative analyses between more chemicals, mixed toxicities, and non-chemical environmental conditions.

STAR★METHODS

Detailed methods are provided in the online version of this paper and include the following:

- KEY RESOURCES TABLE
- RESOURCE AVAILABILITY
  - Lead contact
  - Materials availability
  - Data and code availability
- EXPERIMENTAL MODEL AND SUBJECT DETAILS
  - Worm strains, cultivation, and exposure to pollutants
- METHOD DETAILS
  - Life span assays
  - Mass spectrometry (LC-ESI-MS)
  - Aggregome analysis
  - Microscopy and quantification of polyQ aggregates
  - Microscopy and quantification of DAF-16 localization
  - qPCR
- QUANTIFICATION AND STATISTICAL ANALYSIS

SUPPLEMENTAL INFORMATION

Supplemental information can be found online at https://doi.org/10.1016/j.isci.2022.105027.

AUTHOR CONTRIBUTIONS

A.S. and A.vM. conceived and designed the experiments. A.S., A.L., and KH.G. performed experiments, A.S., A.L., and KH.G. analyzed data, A.S, A.L., KH.G., and A.vM provided scientific input, A.S, and A.vM wrote the article.

DECLARATION OF INTERESTS

The authors declare no competing interests.

REFERENCES

Arnhold, F., Gührs, K.H., and von Mikecz, A. (2015). Amyloid domains in the cell nucleus controlled by nucleoskeletal protein lamin B1 reveal a new pathway of mercury neurotoxicity. PeerJ 3, e754. https://doi.org/10.7717/peerj.754.

Bender, T., Lewrenz, I., Franken, S., Baitzel, C., and Voos, W. (2011). Mitochondrial enzymes are protected from stress-induced aggregation by mitochondrial chaperones and the Pim1/LON protease. Mol. Biol. Cell 22, 541–554. https://doi.org/10.1091/mbc.E10-08-0718.

Ben-Zvi, A., Miller, E.A., and Morimoto, R.I. (2009). Collapse of proteostasis represents an early molecular event in Caenorhabditis elegans aging. Proc. Natl. Acad. Sci. USA 106, 14914–14919. https://doi.org/10.1073/pnas.0902882106.

Chen, M., Singer, L., Scharf, A., and von Mikecz, A. (2008). Nuclear polyglutamine-containing protein aggregates as active proteolytic centers. J. Cell Biol. 180, 697–704. https://doi.org/10.1083/jcb.200708131.

Collins, J.J., Evason, K., Pickett, C.L., Schneider, D.L., and Kornfeld, K. (2008). The anticonvulsant ethosuximide disrupts sensory function to extend C. elegans lifespan. PLoS Genet. 4, e1000230. https://doi.org/10.1371/journal.pgen.1000230.

Corsi, A.K., Wightman, B., and Chalfie, M. (2015). A Transparent window into biology: a primer on Caenorhabditis elegans. WormBook, pp. 1–31. https://doi.org/10.1895/wormbook.1.177.1.

David, D.C., Ollikainen, N., Trinidad, J.C., Cary, M.P., Burlingame, A.L., and Kenyon, C. (2010). Widespread protein aggregation as an inherent part of aging in C. elegans. PLoS Biol. 8. e1000450–48. https://doi.org/10.1371/journal.pbio.1000450.

Forouzanfar, M.H., Afshin, A., Alexander, L.T., Biryukov, S., Brauer, M., Cercy, K., Charlson, F.J., Cohen, A.J., Dandona, L., Estep, K., Ferrari, A.J., et al. (2016). Global, regional, and national comparative risk assessment of 79 behavioural, environmental and occupational, and metabolic risks or clusters of risks, 1990–2015: a systematic analysis for the Global Burden of Disease Study 2015. Lancet 388, 1659–1724. https://doi.org/10.1016/S0140-6736(16)31679-8.

Gems, D., Sutton, A.J., Sundermeyer, M.L., Albert, P.S., King, K.v., Edgley, M.L., Larsen, P.L., and Riddle, D.L. (1998). Two pleiotropic classes of daf-2 mutation affect larval arrest, adult behavior, reproduction and longevity in Caenorhabditis elegans. Genetics 150, 129–155. https://doi.org/10.1093/GENETICS/150.1.129.

Gerhardsson, L., Lundh, T., Minthon, L., and Londos, E. (2008). Metal concentrations in plasma and cerebrospinal fluid in patients with Alzheimer's disease. Dement. Geriatr. Cogn. Disord. 25, 508–515. https://doi.org/10.1159/000129365.

Haghani, A., Dalton, H.M., Safi, N., Shirmohammadi, F., Sioutas, C., Morgan, T.E., Finch, C.E., and Curran, S.P. (2019). Air pollution alters caenorhabditis elegans development and lifespan: responses to traffic-related nanoparticulate matter. J. Gerontol. A Biol. Sci. Med. Sci. 74, 1189–1197. https://doi.org/10.1093/gerona/glz063.

Harris, T.W., Arnaboldi, V., Cain, S., Chan, J., Chen, W.J., Cho, J., Davis, P., Gao, S., Grove, C.A., Kishore, R., Lee, R.Y.N., et al. (2020). WormBase: a modern Model Organism Information Resource. Nucleic Acids Res. 48, D762–D767. https://doi.org/10.1093/nar/gkz920.

Hemmerich, P.H., and von Mikecz, A. (2013). Defining the subcellular interface of nanoparticles by live-cell imaging. PLoS One 8, e62018. https://doi.org/10.1371/journal.pone.0062018.

Henderson, S.T., and Johnson, T.E. (2001). daf-16 integrates developmental and environmental inputs to mediate aging in the nematode Caenorhabditis elegans. Curr. Biol. 11, 1975–1980. https://doi.org/10.1016/S0960-9822(01)00594-2.

Hipp, M.S., Kasturi, P., and Hartl, F.U. (2019). The proteostasis network and its decline in ageing. Nat. Rev. Mol. Cell Biol. 20, 421–435. https://doi.org/10.1038/s41580-019-0101-y.

Honda, Y., Tanaka, M., and Honda, S. (2010). Trehalose extends longevity in the nematode Caenorhabditis elegans. Aging Cell 9, 558–569. https://doi.org/10.1111/j.1474-9726.2010.00582.x.

Janssens, G.E., Lin, X.X., Millan-Ariño, L., Kavšek, A., Sen, I., Seinstra, R.I., Stroustrup, N., Nollen, E.A.A., and Riedel, C.G. (2019). Transcriptomics-based screening identifies pharmacological inhibition of Hsp90 as a means to defer aging. Cell Rep. 27, 467–480.e6. https://doi.org/10.1016/j.celrep.2019.03.044.

Kaletta, T., and Hengartner, M.O. (2006). Finding function in novel targets: C. elegans as a model organism. Nat. Rev. Drug Discov. 5, 387–398. https://doi.org/10.1038/nrd2031.

Kenyon, C., Chang, J., Gensch, E., Rudner, A., and Tabtiang, R. (1993). A C. elegans mutant that lives twice as long as wild type. Nature 366, 461–464. https://doi.org/10.1038/366461a0.

Kenyon, C.J. (2010). The genetics of ageing. Nature 464, 504–512. https://doi.org/10.1038/nature08980.

Kimura, K., Tanaka, N., Nakamura, N., Takano, S., and Ohkuma, S. (2007). Knockdown of mitochondrial heat shock protein 70 promotes progeria-like phenotypes in Caenorhabditis elegans. J. Biol. Chem. 282, 5910–5918. https://doi.org/10.1074/jbc.M609025200.

Kiraly, V.T.R., Dores-Silva, P.R., Serrão, V.H.B., Cauvi, D.M., de Maio, A., and Borges, J.C. (2020). Thermal aggregates of human mortalin and Hsp70-1A behave as supramolecular assemblies. Int. J. Biol. Macromol. 146, 320–331. https://doi.org/10.1016/j.ijbiomac.2019.12.236.

Koyuncu, S., Loureiro, R., Lee, H.J., Wagle, P., Krueger, M., and Vilchez, D. (2021). Rewiring of the ubiquitinated proteome determines ageing in C. elegans. Nature 596, 285–290. https://doi.org/10.1038/s41586-021-03781-z.

Labbadia, J., Brielmann, R.M., Neto, M.F., Lin, Y.F., Haynes, C.M., and Morimoto, R.I. (2017). Mitochondrial Stress Restores the Heat Shock Response and Prevents Proteostasis Collapse during Aging. Cell Rep. 21, 1481–1494. https://doi.org/10.1016/j.celrep.2017.10.038.

Landrigan, P.J., Fuller, R., Acosta, N.J.R., Adeyi, O., Arnold, R., Basu, N., Baldé, A.B., Bertollini, R., Bose-O'Reilly, S., et al. (2018). The Lancet Commission on pollution and health. Lancet 391, 462–512. https://doi.org/10.1016/S0140-6736(17)32345-0.

Lashuel, H.A. (2021). Rethinking protein aggregation and drug discovery in neurodegenerative diseases: why we need to embrace complexity? Curr. Opin. Chem. Biol. 64, 67–75. https://doi.org/10.1016/j.cbpa.2021.05.006.

Lin, K., Dorman, J.B., Rodan, A., and Kenyon, C. (1997). daf-16: an HNF-3/forkhead family member that can function to double the life-span of Caenorhabditis elegans. Science 278, 1319–1322. https://doi.org/10.1126/science.278.5341.1319.

Lin, X.X., Sen, I., Janssens, G.E., Zhou, X., Fonslow, B.R., Edgar, D., Stroustrup, N., Swoboda, P., Yates, J.R., Ruvkun, G., and Riedel, C.G. (2018). DAF-16/FOXO and HLH-30/TFEB function as combinatorial transcription factors to promote stress resistance and longevity. Nat. Commun. 9, 4400. https://doi.org/10.1038/s41467-018-06624-0.

Meleleo, D., Sblano, C., Storelli, M.M., and Mallamaci, R. (2020). Evidence of cadmium and mercury involvement in the Aβ42 aggregation process. Biophys. Chem. 266, 106453. https://doi.org/10.1016/j.bpc.2020.106453.

Mi, H., Muruganujan, A., and Thomas, P.D. (2013). PANTHER in 2013: modeling the evolution of gene function, and other gene attributes, in the context of phylogenetic trees. Nucleic Acid Res. 41, D377–D386. https://doi.org/10.1093/nar/gks1118.

Morimoto, R.I. (2020). Cell-nonautonomous regulation of proteostasis in aging and disease. Cold Spring Harb. Perspect. Biol. 12, a034074. https://doi.org/10.1101/cshperspect.a034074.

Morley, J.F., Brignull, H.R., Weyers, J.J., and Morimoto, R.I. (2002). The threshold for polyglutamine-expansion protein aggregation and cellular toxicity is dynamic and influenced by aging in Caenorhabditis elegans. Proc. Natl. Acad. Sci. USA 99, 10417–10422. https://doi.org/10.1073/pnas.152161099.

Partridge, L., Deelen, J., and Slagboom, P.E. (2018). Facing up to the global challenges of ageing. Nature 561, 45–56. https://doi.org/10.1038/s41586-018-0457-8.

Petrascheck, M., Ye, X., and Buck, L.B. (2007). An antidepressant that extends lifespan in adult Caenorhabditis elegans. Nature 450, 553–556. https://doi.org/10.1038/nature05991.

Pickett, C.L., Dietrich, N., Chen, J., Xiong, C., and Kornfeld, K. (2013). Mated progeny production is a biomarker of aging in caenorhabditis elegans. G3 3, 2219–2232. https://doi.org/10.1534/g3.113.008664.

Piechulek, A., Berwanger, L.C., and von Mikecz, A. (2019). Silica nanoparticles disrupt OPT-2/PEP-2-dependent trafficking of nutrient peptides in the intestinal epithelium. Nanotoxicology 13, 1133–1148. https://doi.org/10.1080/17435390.2019.1643048.

Piechulek, A., and von Mikecz, A. (2018). Life span-resolved nanotoxicology enables identification of age-associated neuromuscular vulnerabilities in the nematode Caenorhabditis elegans. Environ. Pollut. 233, 1095–1103. https://doi.org/10.1016/j.envpol.2017.10.012.

Pillet, B., Mitterer, V., Kressler, D., and Pertschy, B. (2017). Hold on to your friends: dedicated chaperones of ribosomal proteins: dedicated chaperones mediate the safe transfer of ribosomal proteins to their site of pre-ribosome incorporation. Bioessays 39, 1–12. https://doi.org/10.1002/bies.201600153.

Rappaport, N., Twik, M., Plaschkes, I., Nudel, R., Stein, T.I., Levitt, J., Gershoni, M., Morrey, C.P., Safran, M., and Lancet, D. (2017). MalaCards: an amalgamated human disease compendium with diverse clinical and genetic annotation and structured search. Nucleic Acid Research 45,

D877–D887. https://doi.org/10.1093/nar/gkw1012.

Reis-Rodrigues, P., Czerwieniec, G., Peters, T.W., Evani, U.S., Alavez, S., Gaman, E.A., Vantipalli, M., Mooney, S.D., Gibson, B.W., Lithgow, G.J., and Hughes, R.E. (2012). Proteomic analysis of age-dependent changes in protein solubility identifies genes that modulate lifespan. Aging Cell 11, 120–127. https://doi.org/10.1111/j.1474-9726.2011.00765.x.

Roco, M.C. (2003). Nanotechnology: convergence with modern biology and medicine. Curr. Opin. Biotechnol. 14, 337–346. https://doi.org/10.1016/S0958-1669(03)00068-5.

Santra, M., Dill, K.A., and de Graff, A.M.R. (2019). Proteostasis collapse is a driver of cell aging and death. Proc. Natl. Acad. Sci. USA 116, 22173–22178. https://doi.org/10.1073/pnas.1906592116.

Scharf, A., Gührs, K.H., and von Mikecz, A. (2016). Anti-amyloid compounds protect from silica nanoparticle-induced neurotoxicity in the nematode C. elegans. Nanotoxicology 10, 426–435. https://doi.org/10.3109/17435390.2015.1073399.

Scharf, A., Mitteldorf, J., Armstead, B., Schneider, D., Jin, H., Kocsisova, Z., Tan, C.H., Sanchez, F., Brady, B., Ram, N., DiAntonio, G.B., et al. (2022). A laboratory and simulation platform to integrate individual life history traits and population dynamics. Nature Computational Science 2, 90–101. https://doi.org/10.1038/s43588-022-00190-8.

Scharf, A., Piechulek, A., and von Mikecz, A. (2013). Effect of nanoparticles on the biochemical and behavioral aging phenotype of the nematode caenorhabditis elegans. ACS Nano 7, 10695–10703. https://doi.org/10.1021/nn403443r.

Scharf, A., Pohl, F., Egan, B.M., Kocsisova, Z., and Kornfeld, K. (2021). Reproductive aging in Caenorhabditis elegans: from molecules to ecology. Front. Cell Dev. Biol. 9, 718522. https://doi.org/10.3389/fcell.2021.718522.

Scherzinger, E., Lurz, R., Turmaine, M., Mangiarini, L., Hollenbach, B., Hasenbank, R., Bates, G.P., Davies, S.W., Lehrach, H., and Wanker, E.E. (1997). Huntingtin-encoded polyglutamine expansions form amyloid-like protein aggregates in vitro and in vivo. Cell 90,

549–558. https://doi.org/10.1016/S0092-8674(00)80514-0.

Sorrentino, J.A., Sanoff, H.K., and Sharpless, N.E. (2014). Defining the toxicology of aging. Trends Mol. Med. 20, 375–384. https://doi.org/10.1016/j.molmed.2014.04.004.

Streets, D.G., Devane, M.K., Lu, Z., Bond, T.C., Sunderland, E.M., and Jacob, D.J. (2011). All-time releases of mercury to the atmosphere from human activities. Environ. Sci. Technol. 45, 10485–10491. https://doi.org/10.1021/es202765m.

Stroustrup, N., Anthony, W.E., Nash, Z.M., Gowda, V., Gomez, A., López-Moyado, I.F., Apfeld, J., and Fontana, W. (2016). The temporal scaling of Caenorhabditis elegans ageing. Nature 530, 103–107. https://doi.org/10.1038/nature16550.

Tiku, V., Jain, C., Raz, Y., Nakamura, S., Heestand, B., Liu, W., Partridge, L., and Antebi, A. (2017). Small nucleoli are a cellular hallmark of longevity. Nature Communications 8, 16083. https://doi.org/10.1038/ncomms16083.

Tissenbaum, H.A. (2015). Using C. elegans for aging research. Invertebr. Reprod. Dev. 59, 59–63. https://doi.org/10.1080/07924259.2014.940470.

UniProt Consortium (2021). UniProt: the universal protein knowledgebase in 2021. Nucleic Acid Research 49, D480–D489. https://doi.org/10.1093/nar/gkaa1100.

Uversky, V.N., Li, J., and Fink, A.L. (2001). Metal-triggered structural transformations, aggregation, and fibrillation of human α-synuclein: a possible molecular link between Parkinson's disease and heavy metal exposure. J. Biol. Chem. 276, 44284–44296. https://doi.org/10.1074/jbc.M105343200.

Vecchi, G., Sormanni, P., Mannini, B., Vandelli, A., Tartaglia, G.G., Dobson, C.M., Hartl, F.U., and Vendruscolo, M. (2020). Proteome-wide observation of the phenomenon of life on the edge of solubility. Proc. Natl. Acad. Sci. USA 117, 1015–1020. https://doi.org/10.1073/pnas.1910444117.

Vermeulen, R., Schymanski, E.L., Barabási, A.L., and Miller, G.W. (2020). The exposome and health: where chemistry meets biology. Science 367, 392–396. https://doi.org/10.1126/science.aay3164.

von Mikecz, A. (2009). PolyQ fibrillation in the cell nucleus: who's bad? Trends Cell Biol. 19, 685–691. https://doi.org/10.1016/j.tcb.2009.09.001.

von Mikecz, A. (2014). Pathology and function of nuclear amyloid: protein homeostasis matters. Nucleus 5. https://doi.org/10.4161/nucl.29404.

von Mikecz, A. (2018). Lifetime eco-nanotoxicology in an adult organism: where and when is the invertebrate: C. elegans vulnerable? Environ. Sci, Nano 5, 616–622. https://doi.org/10.1039/c7en01061c.

von Mikecz, A., and Scharf, A. (2022). Pollution — bring the field into the lab. Nature 602, 386. https://doi.org/10.1038/d41586-022-00444-5.

von Mikecz, A., and Schikowski, T. (2020). Effects of airborne nanoparticles on the nervous System: amyloid protein aggregation, neurodegeneration and neurodegenerative diseases. Nanomaterials 10, E1349. https://doi.org/10.3390/nano10071349.

Walther, D.M., Kasturi, P., Zheng, M., Pinkert, S., Vecchi, G., Ciryam, P., Morimoto, R.I., Dobson, C.M., Vendruscolo, M., Mann, M., and Hartl, F.U. (2015). Widespread proteome remodeling and aggregation in aging C. elegans. Cell 161, 919–932. https://doi.org/10.1016/j.cell.2015.03.032.

Wang, Y., and Nowack, B. (2018). Dynamic probabilistic material flow analysis of nano-SiO2, nano iron oxides, nano-CeO2, nano-Al2O3, and quantum dots in seven European regions. Environ. Pollut. 235, 589–601. https://doi.org/10.1016/j.envpol.2018.01.004.

Wanker, E.E., Scherzinger, E., Heiser, V., Sittler, A., Eickhoff, H., and Lehrach, H. (1999). Membrane filter assay for detection of amyloid-like polyglutamine- containing protein aggregates. Methods Enzymol. 309, 375–386. https://doi.org/10.1016/S0076-6879(99)09026-6.

Yu, A., Fox, S.G., Cavallini, A., Kerridge, C., O'Neill, M.J., Wolak, J., Bose, S., and Morimoto, R.I. (2019). Tau protein aggregates inhibit the protein-folding and vesicular trafficking arms of the cellular proteostasis network. J. Biol. Chem. 294, 7917–7930. https://doi.org/10.1074/jbc.RA119.007527.

STAR★METHODS

KEY RESOURCES TABLE

REAGENT or RESOURCE	SOURCE	IDENTIFIER
Bacterial and virus strains		
Escherichia coli OP50	Caenorhabditis Genetics Center	WB Strain: OP50 WormBase: WBStrain00041969; RRID:WB-STRAIN:WBStrain00041969
Chemicals, peptides, and recombinant proteins		
$HgCl_2$	Merck	1044190050, CAS: 7487-94-7
$HgCl_2$	Sigma Aldrich	215465-5G
silica NPs, 50 nm	Kisker Biotech	PSi-0.05
BULK silica, 500 nm	Kisker Biotech	PSI-0.5
FUdR (5-Fluoro-2′-deoxyuridine)	Sigma-Aldrich	F0503-250MG, CAS: 50-91-9
Carbenicillin	Merck	69101-3
Fungizone/ Amphotericin B	Thermo Fisher Scientific	15290018
K_2HPO_4	Carl Roth	P749.1, CAS: 7758-11-4
KH_2PO_4	Carl Roth	3904.2, CAS: 7778-77-0
Cholesterol	Sigma-Aldrich	C8667-1G, CAS: 57-88-5
citric acid monohydrate	Sigma-Aldrich	94068-100G, CAS: 5949-29-1
tri-potassium citrate monohydrate	Sigma-Aldrich	25107-1KG, CAS: 6100-05-6
disodium EDTA	Carl Roth	8043.2, CAS: 6381-92-6
$FeSO_4$ x 7 H_2O	Sigma-Aldrich	215422-5G, CAS: 7782-63-0
$MnCl_2$ x 4 H_2O	Sigma-Aldrich	203734-5G, CAS: 13446-34-9
$ZnSO_4$ x 7 H_2O	Sigma-Aldrich	204986-10G, CAS: 7446-20-0
$CuSO_4$ x 5 H_2O	Sigma-Aldrich	469130-5G, CAS: 7758-99-8
$MgSO_4$	Sigma-Aldrich	M7506-500G, CAS: 7487-88-9
$CaCl_2$ x 6 H_2O	Sigma-Aldrich	442909-1KG, CAS: 7774-34-7
Na_2HPO_4 x 2 H_2O	Carl Roth	4984.1, CAS: 10028-24-7
NH_4Cl	Carl Roth	K298.1, CAS: 12125-02-9
Agarose	Sigma-Aldrich	A9539-250G, CAS: 9012-36-6
NaN_3	Sigma-Aldrich	438456-5G, CAS: 26628-22-8
Bacto Agar	BD	214030
Bacto Proteose Peptone No 3	BD	211693
Bacto Yeast Extract	BD	212750
Sodium hypochlorite solution	Carl Roth	9062:3, CAS: 7681-52-9
Protease inhibitor cocktail	Sigma-Aldrich	P2714-1BTL
Guanidinium HCl	Carl Roth	0035.2, CAS: 50-01-1
TRIzol®Reagent	Ambion	15596018
Chloroform	Sigma-Aldrich	319988-500ML
Experimental models: Organisms/strains		
C. elegans: Strain N2	Caenorhabditis Genetics Center	WB Strain: N2 WormBase: WBStrain00000001; RRID:WB-STRAIN:WBStrain00000001

Continued

REAGENT or RESOURCE	SOURCE	IDENTIFIER
C. elegans: Strain DR1572: *daf-2(e1368)* III.	Caenorhabditis Genetics Center	WB Strain: DR1572 WormBase: WBStrain00006381; RRID:WB-STRAIN:WBStrain00006381
C. elegans: Strain CF1038: *daf-16(mu86)* III.	Caenorhabditis Genetics Center	WB Strain: CF1038 WormBase: WBStrain00004840; RRID:WB-STRAIN:WBStrain00004840
C. elegans: Strain AM140: *rmIs132* [unc-54p::Q35::YFP].	Caenorhabditis Genetics Center	WB Strain: AM140 WormBase: WBStrain00000182; RRID:WB-STRAIN:WBStrain00000182
C. elegans: Strain TJ356: *zIs356* IV [daf-16p::daf-16a/b::GFP + rol-6(su1006)].	Caenorhabditis Genetics Center	WB Strain: TJ356 WormBase: WBStrain00034892; RRID:WB-STRAIN:WBStrain00034892
Oligonucleotides		
Primers for *fib-1* Forward: CAAACGTTGTCCCAATTGTCG Reverse: GGAAGTTTTGGGCATTGAGAG	(Tiku et al., 2017)	N/A
Primers for *hsp-6* Forward: GTTATCGAGAACGCAGAAGGAG Reverse: CATCCTTAGTAGCTTGACGCTG	(Labbadia et al., 2017)	N/A
Primers for *hsp-60* Forward: CATGCTCGTCGGAGTCAAC Reverse: TTTGTGATCTTTGGGCTTCC	(Labbadia et al., 2017)	N/A
Software and algorithms		
R, survival analysis, statistics	(Scharf et al., 2022)	N/A
Origin 2022	https://www.originlab.com/	N/A
Excel	Microsoft	RRID:SCR_016137
StepOne Software v2.3	Applied Biosystems/ Thermo Fisher	4376600
Scaffold 4	Proteome Software	N/A
ProteomeDiscoverer 1.4	Thermo Scientific	N/A
Photoshop	Adobe	RRID:SCR_014199
Illustrator	Adobe	RRID:SCR_010279
Other		
QIAprep® Spin Miniprep Kit	QUIAGEN	27104
iScript™	BIO-RAD	1708841
iTaq Universal SYBR® Green Supermix	BIO-RAD	1725121
Silica NPs-induced aggregome	Scharf et al. (2016)	N/A
Aged-induced aggregome	David et al. (2010), Reis-Rodrigues et al. (2012), Walther et al. (2015)	N/A
Proteomic data set	Walther et al. (2015)	N/A

RESOURCE AVAILABILITY

Lead contact

Further information and requests for reagents may be directed to and will be fulfilled by the corresponding author Andrea Scharf (scharfa@uni-duesseldorf.de).

Materials availability

This study did not generate new unique reagents.

Data and code availability

- This paper analyzes aggregome data (see Tables S3 and S6) and existing, publicly available data. The published datasets are listed in the key resources table. All data reported in this paper will be shared by the lead contact upon request.

- This paper does not report original code.

- Any additional information required to reanalyze the data reported in this paper is available from the lead contact upon request.

EXPERIMENTAL MODEL AND SUBJECT DETAILS

Worm strains, cultivation, and exposure to pollutants

C. elegans were cultured at 20°C with *E. coli* OP50 as food source on standard NGM plates or in S-Medium as indicated. For all experiments, nematodes were synchronized by isolating eggs with hypochlorite/NaOH. For lifespans and aged populations, nematodes were cultured with supplemental 5-fluoro-2′-deoxyuridine (FUdR) from L4 larval stage to maintain synchronization and with carbenicillin to arrest bacteria. Nematodes were exposed on adult day 1 (24h after L4) to 0.001, 0.01, 0.02, 0.1, and 1.25 mg/mL 50 nm silica NPs (Kisker, Steinfurt, Germany) or 10, 25, or 50 μM iHg, e.g., mercuric chloride ($HgCl_2$). Silica NPs properties were previously analyzed by dynamic light scattering and live cell imaging and described ((Hemmerich and von Mikecz, 2013); Scharf et al., 2013). The following strains were provided by the Caenorhabditis Genetics Center (funded by NIH Office of Research Infrastructure Programs (P40 OD010440)) and used where indicated: Wild type N2; DR1572 *daf-2(e1368)*; CF1038 *daf-16(mu86)*; AM140 *rmIs132 [unc-54 p::Q35::YFP]* (Morley et al., 2002); TJ356 *zIs356 IV [daf-16p::daf-16a/b::GFP + rol-6(su1006)]* (Henderson and Johnson, 2001). All strains were kept as hermaphrodites without males. Animals were randomly assigned to experimental groups by pipetting random samples.

METHOD DETAILS

Life span assays

Life span assays were performed as previously described (Petrascheck et al., 2007; Piechulek and von Mikecz, 2018). Briefly, approximately ten age-synchronized *C. elegans* were seeded as L1/L2 larvae in 96- well plates containing S-media (including 50 μg/mL carbenicillin and 0.1 μg/mL fungizone) and 6 mg/mL *E. coli* OP50. To maintain worms age synchronized, FUdR was added (1.5 mM final concentration, Sigma) at the L4 larval stage. On adult day 1, worms were left untreated or treated with particles or mercury at concentrations as indicated. Living animals were scored with a dissecting scope. 54–161 worms were tested per group per experiment. Weibull plot was applied to the data of the survival analyses, e.g., curve fitting of the Kaplan-Meier survival curves.

Mass spectrometry (LC-ESI-MS)

Characterization of *C. elegans* aggregomes were performed as previously reported (Arnhold et al., 2015; Scharf et al., 2016). *C. elegans* wild-type animals (N2) were mock (H_2O)-treated or exposed to iHg as indicated on day-1 of adulthood in S-media without FUdR, carbenicillin, and FUdR. Young and aged wild-type *C. elegans* were grown on NGM plates supplemented with FUdR (40 μM) to maintain age-synchronization (Honda et al., 2010). Exposed or young & old nematodes were lysed in SDS-lysis buffer (150mM NaCl, 10mM Tris-HCL pH8, 2% SDS, protease inhibitor) using a swing mill and SDS-insoluble proteins were separated from the soluble protein fraction via filter retardation assay (Scharf et al., 2013). The SDS-insoluble protein fraction was eluted from cellulose acetate membranes with 6M guanidinium hydrochloride (GuaHCl). Dithiothreitol (DTT) was added to the GuaHCl solution to a final concentration of 10 mM and samples were incubated for one hour at room temperature. After addition of iodoacetamide to a final concentration of 20 mM and incubation for one hour at room temperature in the dark, samples were equilibrated to trypsin digestion condition by multiple cycles of ultrafiltration (MWCO = 5000 Da, Microcon, Millipore) and buffer exchange against trypsin digestion buffer (8% acetonitrile in 25 mM ammonium bicarbonate). The sample solutions were digested with 15 ng trypsin overnight, dried in a rotary evaporator, dissolved in 20 μL 0.1% formic acid (FA) in 5% acetonitrile, centrifuged for 2 min (14,000 rpm) and

the supernatants were transferred to a polypropylene-sample vial. Five μL of each sample were analyzed by MS and where necessary the remaining 15 μL were used for one additional measurement.

For mass spectrometry, the LTQ Orbitrap XL ETD (Thermo Scientific) coupled to a nano-HPLC NanoLC 2D System AS 1 (Eksigent) was used. The samples were loaded onto a trap column (Robust Reversed Phase Solid Phase Extraction Trap 100 μm × 40 mm, NanoSeparations) and washed with 30 μL buffer A (5% acetonitrile/0.1% formic acid). The bound analytes were transferred to a separation column (75 μm × 100 mm, NanoSeparations) by applying a linear gradient from 0 to 38% of buffer B (80% acetonitrile/0.1% formic acid) over 76 min.

The measured spectra (DDA, top 8, ion trap) were processed by ProteomeDiscoverer 1.4 (ThermoScientific) and searched against the SwissProt (December 2015) database by Mascot (MatrixScience). The following search parameters were used in all searches: enzyme - trypsin with two allowed miss cleavages; fixed modification - carbamidomethylation of cysteine; variable modification - oxidation of methionine, phosphorylation of serine and threonine; measurement precision of precursor ions - 10 ppm; measurement precision of fragment ions - 0.5 Da.

Data compilation was performed by Scaffold 4 (Proteome Software) using the Mascot dat files and the msf files of ProteomeDiscoverer 1.4 of the measurements. The following parameters were used for the evaluation by Scaffold: Protein Grouping Strategy: Experiment-wide grouping with binary peptide-protein weights, Peptide Thresholds: 95,0% minimum, Protein Thresholds: 99,0% minimum and 2 peptides minimum, Peptide FDR: 0,0% (Decoy), Protein FDR: 0,0% (Decoy).

Aggregome analysis

For the age-induced aggregome, proteins that were identified in 2 out of 4 biological replicates were subjected to further analysis (Table S6), whereas for the iHg-induced aggregome, proteins identified in the 3 biological replicates were pooled (Table S3). Identification and analysis of candidates for the silica NPs-induced aggregome were previously reported (Scharf et al., 2016). For further characterization, the identified aggregome candidates were analyzed by data mining of the following databases: PANTHER (Mi et al., 2013), UniProt (UniProt Consortium, 2021), and WormBase (Harris et al., 2020), and MalaCards (Rappaport et al., 2017). Specifically, each identified insoluble protein was categorized according to its biological process classified using the PANTHER database, UniProt, WormBase, and literature. Structural protein feature were analyzed as previously described (Arnhold et al., 2015). Briefly, structural feature information for each aggregome network were extracted from the UniProt database and percentage of aggregome network proteins with beta-strands, coiled-coil, cross-link, DNA binding, disulfide bonds, helices, metal binding feature, nucleotide binding feature, repeats, and zinc fingers was calculated, respectively. Then, statistical over- or underrepresentation was calculated by comparing to the average percentage of proteins in the total *C. elegans* genome with each feature.

For the comparative MS data analysis of aged aggregomes, SDS- insoluble data sets from two previously publications (David et al., 2010; Reis-Rodrigues et al., 2012) were compared to the identified age-induced aggregome network of this study (Tables S4 and S5). In addition, the proteomic data set published in (Walther et al., 2015) were used for analysis of protein abundances.

Microscopy and quantification of polyQ aggregates

C. elegans expressing repeats of 35 glutamines fused to yellow fluorescent protein in body wall muscle cells (AM140 *rmIs132* [unc-54 p::Q35::YFP] (Morley et al., 2002) were exposed to iHg or mock(H$_2$O)-treated on adult day 1 in the presence of carbenicillin and FUdR. After 24 h, living hermaphrodites were imaged on 5% agarose pads/10 μM NaN3 with a 60×/1.4NA Plan Apo objective. Fluorescence quantifications was performed as described previously (Scharf et al., 2016).

Microscopy and quantification of DAF-16 localization

C. elegans expressing DAF-16 fused to green fluorescent protein (TJ356 zIs356 IV [*daf-16p::daf-16a/b::GFP + rol-6(su1006)*]) were transferred as L4 larvae in liquid medium on 96-well plates containing 12 mg/mL *E. coli* OP50. Nematodes were treated with FUdR (1.5 mM final concentration) to prevent self-fertilization in the absence of carbenicillin. Silica NPs and iHg were added on day 1 of adulthood at the indicated concentrations. For nuclear translocation scoring, animals were analyzed 24 h after exposure. To induce

heat stress, worms were kept at 37°C for 15 min in a water bath. Living hermaphrodites were placed on 5% agarose pads with 10 μM NaN3 at room temperature and analyzed by epifluorescence microscopy with a 60×/1.4 NA Plan Apo objective (I×70, Olympus, Tokyo, Japan). Micrographs were taken with a stereo microscope (SMZ18, Nikon Europe B.V., Amsterdam, Netherlands) with a SHR Plan Apo 2× objective. GFP fluorescence was detected by 488 nm excitation/510–550 nm emission. Worms showing DAF-16 translocation to the nucleus of intestinal cells were scored as nuclear DAF-16 localization. Per treatment per experiment, 20–33 worms (n) were tested. All experiments were performed at least four times.

qPCR

C. elegans wild-type (N2) animas were transferred as L4 larvae in liquid medium in 6-well plates containing 6 mg/mL *E. coli* OP50. Nematodes were treated with FUdR (1.5 mM final concentration) to prevent self-fertilization. iHg were added on day 1 of adulthood at the indicated concentration. Animals were transferred into 2 mL RNase free Eppendorf tubes and washed with M9. After the last wash step, the supernatant was discarded. 400 μL TRIzol®Reagent was added to the 100 μL pellet and 5× snapped freezed in liquid nitrogen/thawed at 37°C. Additional 200 μL TRIzol®Reagent were added, incubated for 5 min at room temperature, and followed by the addition of 140 μL chloroform. Samples were shaked for 15 s, incubated for 2 min, and spun down for 15 min at 12000 g at 4°C. After removal of the upper aqueous phase, RNA isolation was finished using the QIAprep® Spin Miniprep Kit (step 5–12, animal tissue section). RNA was transcribed in cDNA via iScript (BIO-RAD). Finally, primers, SYBR® Green supermix, and cDNA (final 20μL) were mixed in MicroAmp Fast Optical 96 well reaction plates and loaded onto the thermal cycler.

QUANTIFICATION AND STATISTICAL ANALYSIS

Quantification described in sections: Microscopy and quantification of polyQ aggregates and Microscopy and quantification of DAF-16 localization. Statistical tests were performed using R and Origin. Student's t test, one-way ANOVA followed by a Tukey post-hoc test, or log rank test was used to determine statistical significance with a p value below 0.05. Details to the statistical tests are provided in the respective figure legends and in Table S1. The two parameters for the Weibull distribution were estimated to fit median survival function. Sample sizes with numbers between 20-160 were chosen based on standard *C. elegans* procedures.